Characterizing major avalanche episodes in space and time in the twentieth and early twenty-first centuries in the Catalan Pyrenees

Pere Oller[1], Elena Muntán[2], Carles García-Sellés[1], Glòria Furdada[2], Cristina Baeza[3], Cecilio Angulo[3]

[1] Institut Cartogràfic i Geològic de Catalunya, Barcelona, Catalonia, Spain.

[2] Universitat de Barcelona, Barcelona, Catalonia, Spain.

[3] Universitat Politècnica de Catalunya, Barcelona, Catalonia, Spain.

Abstract

With the aim of better understanding avalanche risk in the Catalan Pyrenees, the present work focuses on the analysis of major (or destructive) avalanches. For such purpose major avalanche cartography was made by an exhaustive photointerpretation of several flights, winter and summer field surveys and inquiries to local population. Major avalanche events were used to quantify the magnitude of the episodes during which they occurred, and a Major Avalanche Activity Magnitude Index (MAAMI) was developed. This index is based on the number of major avalanches registered and its estimated frequency in a given time period, hence it quantifies the magnitude of a major avalanche episode or winter. Furthermore, it permits a comparison of the magnitude between major avalanche episodes in a given mountain range, or between mountain ranges, and for a long enough period, it should allow analysis of temporal trends. Major episodes from winter 1995/96 to 2013/14 were reconstructed. Their magnitude, frequency and extent were also assessed. During the last 19 winters, the episodes of January 22-23 and February 6-8 in 1996 were those with highest MAAMI values, followed by January 30-31, 2003, January 29, 2006, and January 24-25, 2014. To analyze the whole twentieth century, a simplified MAAMI was defined in order to attain the same purpose with a less complete dataset. With less accuracy, the same parameters were obtained at winter time resolution throughout the twentieth century. Again, 1995/96 winter had the highest MAAMI value followed by 1971/72, 1974/75 and 1937/38 winter seasons. The analysis of the spatial extent of the different episodes allowed refining the demarcation of nivological regions, and improving our knowledge about the atmospheric patterns that cause major episodes and their climatic interpretation. In some cases, the importance of considering a major avalanche episode as the result of a previous preparatory period, followed by a triggering one was revealed.

Key words

Major avalanche, major avalanche episode, Pyrenees, magnitude, frequency, hazard, risk.

1 Introduction

At mountain areas that receive frequent large storms, the 10-year and the 100-year avalanche in a particular path may be similar in size. In contrast, in some generally low-snowfall areas, the 100-year avalanche may be many times larger than the 10-year avalanche. The historical record or the damage to vegetation provide good evidence of avalanche potential in the heavy-snowfall locations, while the low-snowfall locations require extensive applications of indirect techniques to determine the size of the long-return-period event (Mears, 1992).

The Catalan Pyrenees, especially in its southern side present a low and irregular snowfall regime (García et al., 2007). In this region, migration of people from mountainous areas to cities during the sixties and seventies of the last century caused a major human dispersal and thus difficulty in finding historical memory. These factors make that avalanche risk, due to low frequency avalanches, still presents many unknowns despite being significant. In any case, either through surveys to the Pyrenean population, or through searching in historical archives, nowadays we know that in Catalonia there are at least 11 villages that have historically been affected by avalanches (Rodés and Miranda, 2009; Avalanche Database of Catalonia, BDAC), some of which almost completely destroyed (Gessa, 1444; Tavascan-Plau, 1604; Àrreu, 1803), and numerous isolated houses, affected or destroyed. Furthermore there are frequent episodes of lower intensity affecting mountain infrastructures (e.g. roads, ski resorts, power lines) every winter. This high frequency activity is what causes victims in winter sports (about 1.5 fatalities per average winter in the Pyrenees of Catalonia, Martinez and Oller, 2004).

Knowing how often major episodes occur, their intensity, and their tendency through time, in relation to climate variability, are basic questions to better understand hazard and to manage avalanche risk in this mountain range.

Different works have dealt with the characterization of major avalanche episodes in the Pyrenees, from different points of view. Esteban et al. (2005) relate the avalanche activity to the snowfall regime and characterize the different synoptic circulation patterns that can generate fresh snow depths susceptible to produce avalanches from a set of 15 years. Garcia-Sellés et al. (2007 and 2009) proposed the study from the analysis of atmospheric circulation associated with the occurrence of major avalanches documented through monitoring and surveillance. From episodes identified during the past 40 years, they determined and classified which are the atmospheric configurations that generated them, and they obtained the probability of occurrence for each one of the regions established for the regional avalanche forecasting. Finally, Muntán et al. (2004 and 2009) identified new events from dendrochronological analysis of tree rings from trees affected by avalanches, from which they reconstructed major episodes and determined their triggering atmospheric and snowpack conditions over the past 40 years. They also identified probable events up to 100 years ago.

Extensive work has been performed in the French Alps (Eckert et al., 2010b; 2013) and the French Pyrenees (Eckert et al., 2007; 2010a; 2013; Eckert, 2009), with observational avalanche data obtained from the EPA (Enquête Permanente sur les Avalanches). Avalanche events from around 3900 paths were systematically recorded since the beginning of the 20^{th} century. The main goal of this work was to analyze avalanche activity throughout time and space in order to determine trends or changes, and its possible relation with climate change, from the use of advanced statistical procedures. Two periods showing different trends were determined during the last 60 years with a change point around 1978 and a retreat of avalanche runouts over the last 61 winters for high magnitude events, although the probability of a high magnitude event has remained constant, suggesting that climate change has recently had little impact on the avalanching rhythm in France.

Studies in other mountain ranges based on avalanche records as quantifiers of the magnitude of avalanche episodes, do establish indexes (e.g. Avalanche Activity Index, AAI) to quantify the daily degree of activity or the degree of activity for a greater period of time with variable accuracy depending on the available data (Schweizer et al., 1998; Laternser and Schneebeli, 2002; Haegeli and McClung, 2003; Eckert et al., 2010a). Others (Germain et al., 2009), used similar indexes to quantify avalanche activity identified from dendrochronological analysis. In all these works the methodology and scale of work is adapted to the completeness and quality of the database used in each case.

In the present work, we analyzed individual major avalanches to quantify the magnitude and frequency of major avalanche episodes in the Catalan Pyrenees. We considered a "major avalanche" (MA) as the avalanche which extent exceeds the reach of the usual (frequent) avalanches, causing damage in case there is forest or infrastructures in the vicinity (Schaerer, 1986). These avalanches have been described as destructive by Schneebeli et al (1997) and specifically catastrophic when they affect villages and cause damage to property (buildings, roads and other infrastructures; Höller, 2009). We observed that these avalanches typically have a return period over 10 years. We considered a "major avalanche episode" (MAE) as the period in which the release of one or more MA occurs due to snowpack instability generally caused by a severe storm with high snowfalls accompanied by substantial drifting snow, but also temperature variations causing snowmelt and or fluctuations of the freezing level, designated as “avalanche cycle” by other authors (Höller, 2009; Eckert et al., 2011). It can last from a few hours to several days. It’s relation to climatic factors makes its study highly valuable to improve avalanche forecasting (Birkeland et al., 2001; García et al., 2009; Eckert et al., 2011).

We worked with MA because they cause damage and therefore risk, and because this fact allows collecting a complete data set of avalanches obtained from a threshold defined by the observed damage, as applied by Fitzharris (1980).

The objectives of this paper are: (i) to reconstruct major avalanche episodes occurred over the Pyrenees of Catalonia during the twentieth and early twenty-first century, (ii) to determine their magnitude, (iii) frequency, and (iv) spatial extent.

The rest of the paper is organized as follows. Section 2 presents the main particularities to consider in relation to the avalanching process and climatic behavior of the study area. Section 3 describes the data set used for this work and how it was treated. Section 4 analyses MAE from time and space point of views considering two temporal periods according to data accuracy. Section 5 discusses the obtained results while section 6 summarizes the main outcomes of the work.

2 Study area

The study area comprises the Catalan Pyrenees, or southeastern part of the Pyrenean range (Figure 1), an area of 5000 km^2. The highest peaks just exceed 3000 m a.s.l. Where the terrain is prone to avalanche release, avalanches can trigger from above 1400 m a.s.l., and they can reach elevations as low as 600 m a.s.l. (Oller et al., 2006). In this area, the Cartographic and Geological Institute of Catalonia (ICGC) carries out an observation and surveillance survey from which avalanche data is added in the Avalanche Database of Catalonia (BDAC, Oller et al., 2005).

The forest, widespread all across the range, plays a key role in the detection of MA. The timberline oscillates between 2100 and 2500 m a.s.l. (Carreras et al., 1996). Above these elevations, the density of trees decreases dramatically to a point (treeline) from which only some individuals develop as a bush. Trees act as sensors that record any disturbance or impact affecting their growth. The effects remain for years and can be used to map avalanches even after the disappearance of the avalanche deposit. Therefore, their mapping can be more systematic than the mapping of avalanches that have not caused destruction to forest. Avalanches that affect human settlements and infrastructures were also considered, but vulnerable elements are distributed irregularly and sometimes they are variable in time, and this fact makes the analysis more complex.

High-frequency avalanches generally occur above the timberline. Currently it is not possible to get a systematic record of such avalanches, as observations are made mainly from fixed points covering small areas of the territory, or they are registered selectively in case of accident. They are impossible or very difficult to detect after the thaw if they don’t produce any further evidence. In addition, even low-frequency avalanches releasing and arriving above the timberline are very difficult to detect after the thaw. For that reason, these areas, glacial cirques and hanging valleys above 2000 m, were considered areas without information, or blind areas (shaded in green in Figure 1). In these areas it was not possible to obtain an exhaustive inventory of major avalanches.

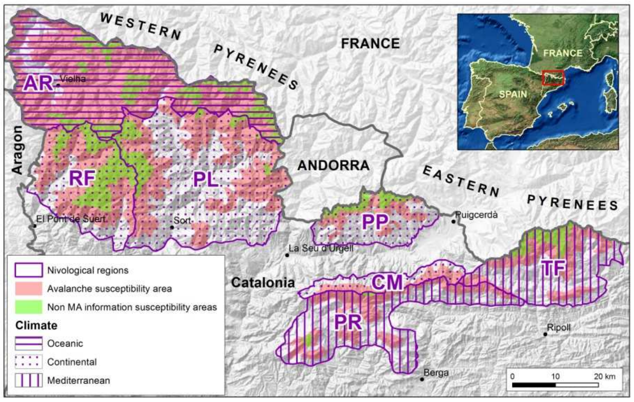

Figure 1. Location of the Catalan Pyrenees. Nivological regions are demarcated by violet boundaries: AR (Aran-Franja nord de la Pallaresa), RF (Ribagorçana-Vall Fosca), PL (Pallaresa), PP (Perafita-Puigpedrós), CM (Vessant nord del Cadí-Moixeró), PR (Prepirineu), TF (Ter-Freser). Areas susceptible to avalanche activity (shaded in red). Areas without MA information (shaded in green). Climate varieties identified by García et al., 2007.

In 1990 the study area was divided into 8 nivological regions (NR) for operational forecasting (García et al., 1996). In 1994 these regions were reduced to 7 (Figure 1). This division was based on climate characteristics, snowpack evolution and avalanche activity (García-Sellés et al., 2007) for a better characterization of the snow conditions and for a better communication of the avalanche forecasting bulletin (BPA). Hence, it was the empirical result of 20 years of avalanche forecasting. It is not a climatic classification in a strict sense, because at present meteorological data series are not long enough to support it (García-Sellés et al., 2007). These regions are Aran-Franja nord de la Pallaresa (AR), Ribagorçana-Vall Fosca (RF), Pallaresa (PL), Perafita-Puigpedrós (PP), Vessant nord del Cadí-Moixeró (CM), Prepirineu (PR), Ter-Freser (TF). All the regions drain their waters towards the Mediterranean sea with the exception of the western half of AR which drains towards the Atlantic ocean.

Three climate varieties were defined (García-Sellés et al., 2007). The north-western part has a humid oceanic climate with regular winter precipitation (AR region). The total amount of new snow is about 500-600 cm in winter and the winter average temperature is -2.5°C at 2200 m a.s.l.. Towards the south of the western Catalan Pyrenees (RF, PL, PP and CM regions), the weather gains continental traits, and winter precipitation decreases. The average new snow depth at 2200 m a.s.l. is 250 cm in winter and the average temperature is -1.3°C. The prevailing winds are from the north and northwest, and they are more intense than in the oceanic domain, often with gusts over 100 km/h. In the eastern Pyrenees the Mediterranean influence takes predominance. Winter precipitation increases though irregularly distributed (PR and TF regions) and it is linked to Mediterranean cyclogenesis. The prevailing winds come from north and highest gusts often exceed 200 km/h at 2000 m a.s.l. The total amount of new snow at 2200 m a.s.l. is about 350-450 cm and winter average temperature is -0.8°C.

García-Sellés et al (2009) identified the atmospheric patterns which generate MAE over the Pyrenees of Catalonia. They worked with 25 episodes from 1972 to 2007 (35 winters), obtaining 6 atmospheric patterns at synoptic scale at a geopotential height of 500 hPa that cause major avalanche episodes (Table 1). They observed that the most common pattern (39% of variance) were north and northwest advections. The 2nd and 3rd patterns, significantly similar to middle and low levels (east and southeast advections), occurred with a frequency of 31%. The other patterns have a lower frequency and they constitute the remaining 25%. This classification was used in the present work to analyze the selected MAE.

Table 1. Synthesis of the atmospheric patterns defined by García-Sellés et al (2009)

Component	500 hPa synoptic configuration	Low levels synoptic configuration	No. of episodes	Snow and avalanche conditions	Typical NR	Acronym
1	Azores high pressures extended over the Atlantic Ocean and deep low pressure on the axis Baltic Sea-Italian Peninsula	N and NW advection	12	Intense snowfalls, very low temperature, very active snowdrift. Major powder avalanches, sometimes wet.	AR	N/NW
2	Long trough at 500 hPa exhibiting an oblique axis oriented NW–SE, due to the Siberian high over Europe which diverts troughs to the Mediterranean Basin	Low pressures, SE flow	4	Weak layers in the snowpack. Heavy precipitation. Dense flow avalanches	PR, TF	E/SE1
3	A blocking high pressures situation at 500 hPa over Central and North-Western Europe and a cut-off low centered over the south of the Iberian Peninsula–North of Africa	High pressures, E and SE advection	4	Intense snowfalls, mild temperatures. Dense and wet avalanches	PR, TF, RF	E/SE2
4	A deep low with a very cold core over the Lion Gulf	N and NE advection	1	Strong northern winds and heavy snowfalls. Major powder avalanches	Any region	CL
5	A wide low pressure is located at high and low levels in the west of the Iberian Peninsula	S and SW advection	2	Very intense precipitation, mild temperatures. Dense dry and wet avalanches	PR, CM, RF, TF	S/SW
6	A ridge from the subtropical anticyclonic belt spreads further north over the Western Mediterranean Sea	Worm advection	2	Sudden melting processes on snow cover which contains persistent weak layers	Any region	A

3 Material and methods

3.1 Major avalanche data

We worked with avalanches recorded in the BDAC of the ICGC (Oller et al., 2005). Data were collected over the past 25 years. Currently the BDAC stores 3052 avalanche observation (AO) records, dated from 1971 to present, and 459 avalanche enquiry (AE) registers (called generically avalanche enquiries although they include enquiries –oral- information s. s. and also historical documentation) from the Middle Ages to 1997. In the BDAC, each register is mapped and different qualitative and quantitative data are recorded (release date and conditions, morphometrics, flow characteristics, damage). AO data come from the ICGC observation network created in 1988 (Furdada et al., 1990) and AE data come from systematic field surveys performed from 1986 to 2006 to elaborate the Avalanche Paths Map (Oller et al., 2006) even though nowadays if new findings are made they get recorded likewise.

For this study an extra effort was done to complete and improve the MA data of the BDAC. Specially, the photointerpretation of different flights with complete coverage of the Catalan Pyrenees was reinforced. Moreover, additional work was done to prepare data for treatment: (i) selection of major avalanches, (ii) debugging data to avoid mistakes and repetitions and (iii) completing the series from field work, inquiries to population and photointerpretation.

Altogether, we used a dataset consisting of 654 major avalanches, 477 of which dated, at least, at winter season resolution, and the rest, dated with less accuracy.

Avalanche information was obtained through various sources (Figure 2): (i) event observation, (ii) photointerpretation, (iii) historical information and (iv) dendrochronology. Each source contributes in a different manner, these being complementary sources (Ancey, 2004; Corona et al., 2012), the joint use of which improves the reconstruction of the registered avalanches. An outline of advantages and drawbacks depending on the source is given further below.

Based on the completeness of the series, we defined 3 periods: (i) P1, with very sporadic records prior to the twentieth century obtained from historical documents largely. Usually they are isolated events that affect localities. The oldest events are dated to the fifteenth century. The length of the runout of most of these avalanches has not been repeated since then. The MA register has not have enough continuity to be used in the time analysis, but the runout distance of these avalanches have interest as a reference distance in relation to the length of other avalanches, all in the same avalanche path, as in the corresponding NR. (ii) P2, which covers the twentieth century, until winter 1994/95. Mostly, the record was obtained from inquiries to the local population, but also from dendrochronological analyses (Muntán et al., 2004 and 2009). The dataset is incomplete but probably the most important events were recorded. P3 (iii), from winter 1995/96 to the present, the record of MA can be considered systematic and complete. Avalanches were mapped from the observation of phenomena and evidence on the vegetation and infrastructures.

Although there are records since the 15th century (P1) in the dataset, we worked with P2 and P3 data as it was considered that the series were reasonably complete with respect to the episodes of greater magnitude (Figure 2).

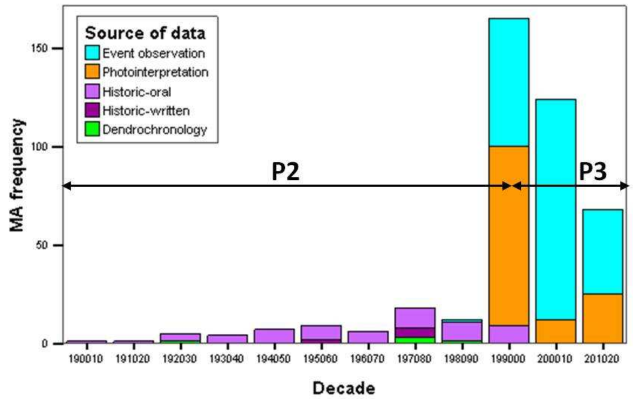

Figure 2. Decadal distribution of MA (Major Avalanches) recorded, and source of the data in P2 and P3 periods. Date of winter has the format $Y_1Y_1Y_1Y_1Y_2Y_2$, where $Y_1Y_1Y_1Y_1$ is the year in which the winter season starts, and Y_2Y_2 identifies the consecutive year.

3.1.1 Event observation

Events can be mapped from direct observation of their effects during winter or from effects on vegetation or infrastructures once winter is over. We call terrain mapping the group of methods used to map avalanches through their effects. In MAE, during winter, the large number of fallen avalanches requires a good mapping strategy, because the lapse of time before avalanche deposits disappear might be short or weather conditions can be adverse to carry out the task. So, when possible, helicopter flights were done just after the MAE in order to obtain an overview of the extent of the episode and the released avalanches and to take photos. This previous work allowed a prioritization for subsequent mapping in the field of the most important avalanches; while the remaining avalanches were mapped from the pictures taken from the air. The mapping of the avalanche in the field increased the accuracy of the observations made from the air.

All this procedure was possible, on the one hand, if there were appropriate flying conditions (visibility and good wind conditions) and good accessibility over land to the avalanche sites, and, on the other hand, if subsequent snowfalls, drifted snow accumulations or high temperatures, had not altered the deposit conservation, hindering its identification. Orthoimages and topographic base 1:5000 were used as reference maps, as well as GPS, allowing to georeference all field observations accurately up to reaching metric resolution. For smaller magnitude MAE, the work was done exclusively over land.

Temporal accuracy of the data is often at episode resolution (daily or almost daily). Normally, although we have no accurate temporal information of all avalanches recorded, episodes can be reconstructed from the analysis of the avalanche characteristics and their spatial distribution. Spatial resolution is variable. If the cartography was made from an oblique photo, and not many references (trees, rocks, forms) could be identified on the landscape, the error could be up to 100 m. Besides, if there were good references, the error could be reduced to around 10 m. If the cartography was done in the field by using a high precision GPS, error was less than 10 m. However, for events involving very dry and non cohesive snow, with a powder part, the furthest point of the runout is sometimes impossible to locate because of the low definition of the deposit (Eckert et al., 2010a).

Summer field work after avalanche occurrence was always necessary, even though the avalanche had been mapped in winter. When the avalanche was destructive, especially to forest, it was mapped during summer from the damage to trees. In addition, conditions for accessing to the site are better and there is not the haste of the winter inspection. Evidence may be diverse, but mapping mostly relies on the external signs that avalanches have left on vegetation.

In addition, it is possible to map the boundaries of the affected area several years after if there is dead wood. Tree remains can last around 10 years at least before they disappear by decay (Elena Muntán, personal observations). The degradation rate of dead wood depends on moisture, temperature and species. As a general rule, humidity and average temperature is lower as we ascend in the Pyrenees and thus, tree wood debris lasts longer at high altitudes. *In situ* stumps of resinous conifers can last appreciably longer. These are, however, the limits of the avalanche destruction, and it is not possible to clearly distinguish the damage caused by the dense part of the avalanche from the powder part, if a mixed avalanche took place. Only when the avalanche occurred the winter before the field inspection, it was still possible to see the scattered twigs carried by the powder part and map the limits of the area. At this stage, mapping from evidence provided information exclusively from the track and the runout of the avalanche path. When using a high resolution GPS the georeferenciation accuracy can be very good (10 to 1 m), but if evidences are not clear, the identification of the limits of the avalanche can be more imprecise.

3.1.2 Photointerpretation

The analysis of aerial photographs guaranteed the completeness of the MA cartography, given its geographical extent and precision. Photointerpretation was used to search for evidences of MA not detected from event observation, to complement the information obtained from other sources. By comparing aerial photographs before and after the episodes, not only the avalanches that had destroyed the forest could be mapped, but also the extent of the devastated forest could be quantified. In addition, by this method, it was possible to examine the whole of the affected territory quickly and economically. The first available flight covering the Catalan Pyrenees in a digital format is the “American flight” performed from 1956 to 1957. The second digital flight covering this region was done 33 years later (1990), but the frequency of new flights has increased up to present, with flights from the Cartographic and Geological Institute of Catalonia (ICGC) almost every year. This fact allows a very detailed monitoring of recent activity.

The temporal accuracy of data depends on the frequency of the successive flights. In any case, the current resolution is, at best, the winter season. However, depending on the distribution and characteristics of MAE occurrence during the time window without ortoimages, some events can be dated at episode resolution. This resolution decreases very fast as we go back in time because the spacing between flights increases rapidly. The combined use of the other information sources improves the dating of the observed events. The spatial resolution depends on the images resolution, which has been improved from the first flights available (scale 1:33.000), to the recent flights (mainly 1:5.000), then obtaining a metric resolution when mapping. For dense flow avalanches, with a well defined deposit, the accuracy can be metric using recent aerial images. In the case of avalanches with a powder part, the precision is lower, obtaining a boundary corresponding to the extent of the avalanche with destructive capacity. Photointerpretation should always be supported by field observation in order to get a better accuracy.

3.1.3 Historical information

A basic source of historical information is the survey to people living in the affected areas, preferably the elderly, which allows obtaining information of a longer time period. This technique revealed the occurrence of avalanches during the twentieth century, mainly. Enquiry data is not continuous and systematic, and the information provided by respondents is often inaccurate, and in some cases wrong (Ancey, 2006). However, sometimes this information can be refined by other sources. In any case, this information has improved significantly the knowledge of avalanche activity during the twentieth century (P2 period).

Temporal accuracy of recounted avalanches is often very imprecise. Only 23% of the registered events were dated to winter season resolution. The spatial accuracy is very variable also; it is generally possible to know the place affected by the avalanche, but not its actual limits.

Search in historical archives and documents directly or indirectly provided evidence of the occurrence of avalanches. This technique allowed us to find events before the twentieth century. It is a very time-consuming and specialized method because it requires the review of a large amount of documentation to find little information. But whatever data found is important because normally, if the avalanche was recorded, it is because it caused damage.

By contrast to other sources, the exact date of the event occurrence is often found in historical records, being the time resolution, daily. The spatial accuracy is very variable, because usually information describes where the damage was, but it is hard to know the actual reach of the avalanche. In general, the obtained information should be considered as a minimum distance in the runout. Even more difficult is to get information of the starting zone.

Note also that historical data are usually biased towards events that have caused damage to structures or loss of life on the one hand, and non-existent in areas depopulated on the other (Corona et al., 2012).

3.1.4 Dendrochronology

Dendrochronology provides data about frequency and extent of avalanche events from the analysis of tree rings. It is therefore necessary that there is forest in the vicinity of the avalanche path. Samples from trees are collected and analysed using prevailing dendrogeomorphological methods such as described by Stoffel (2013). Especially, growth-disturbed trees located in the lower track and runout were analysed to find out high-magnitude events reaching the largest distances. In every avalanche path, we used reference chronologies (Stokes, 1968) built from undisturbed trees in the nearby forest to verify datings. Events can be dated with annual resolution by this technique and the time interval depends on tree age, data ranging from the oldest evidence to the present. From a spatial point of view, depending on the sampling effort, a resolution of the order of 10 m can be obtained. Thus, we included data from dendrochronology in the dataset in the few cases where there was enough information related to runout extent (Muntán et al., 2004, 2009).

3.2 Major avalanche data characterization

We worked with data from 654 MA registered in 515 avalanche paths. In Figures 3, 4 and 5 some characteristics of these MA are compared with all the avalanche observations (AO) registered in the BDAC. Avalanche observations are mainly avalanches that cause winter sports accidents and affect roads, ski resorts, infrastructures, buildings, etc., or occur close to them, they are gathered from fixed observation points and they include artificially released avalanches. They permit comparison of a random sample of avalanches documented since 1971 until today (AO), with MA, a selected set of naturally released avalanches that comply with Schaerer definition as explained in previous sections. It is necessary to clarify the term "random" because if AO are recorded it is because they have caused some disturbance in human activity. Although deviations from random are expected because of the existence of avalanches triggered artificially, different periods of observation depending on the observer or the affected infrastructure, etc., these are not dealt with in this study. Here AO data have only been used for comparison with MA data.

As shown in Figure 3, major avalanches are medium to large size avalanches (sizes 3 and 4 mainly, according to the Canadian snow avalanche size classification system, McClung and Schaerer, 2006), with remarkable destructive capacity. But small size avalanches can also be considered MA if they caused damage as indicated in figure 3. Clearly MA are infrequent avalanches, as can be seen using AO distribution as the reference distribution. Interestingly, proportions among MA are similar to those found out by Barbolini and Keylock (2002) for a single avalanche path (Sudavik avalanche path, Iceland; classes 3+3.5, 45%, and classes 4+4.5, 50% in their case), when explaining which are the most frequent avalanche sizes reaching an extreme runout.

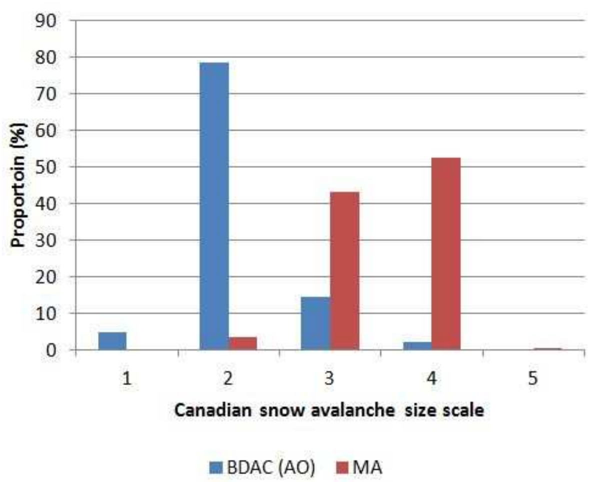

Figure 3. Size of documented Major Avalanches (MA, n = 528 out of 654) and size of avalanches observed and documented in BDAC since 1971 (BDAC-AO, n = 2054 out of 3052) according to the Canadian snow avalanche size scale (McClung and Schaerer, 2006).

Regarding the type of observed dynamics (Figure 4), major avalanches are mostly avalanches in which a powder part (aerosol) has been observed (purely powder or mixed ones). They are drier and therefore lighter, faster and more powerful than regular avalanches, which are mostly wet snow ones.

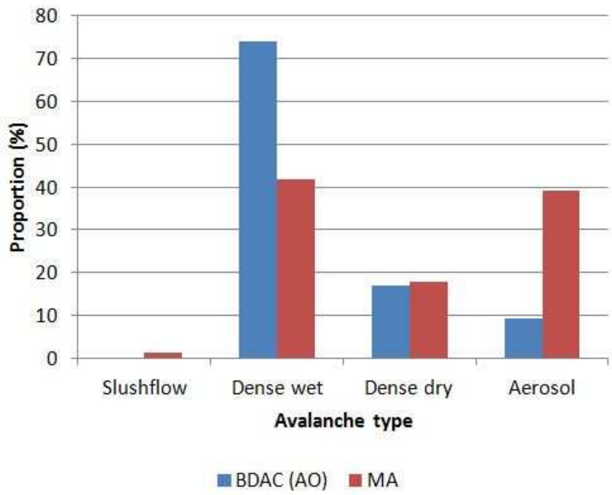

Figure 4. Type of Major Avalanche dynamics (MA; n=223 out of 654) in relation to Avalanche Observation registered in the BDAC since 1971 (BDAC-AO; n=1371 out of 3052).

This behavior is due to the fact that occurrence of the episodes is registered mainly in January, in a very marked peak, decreasing logarithmically towards May (figure 5), being January and February the coldest months in the Catalan Pyrenees (SMC, UB, ICC, 1997). It explains why MA are mainly dry (57%) and often present a powder part (39%). AO are more uniformly and normally distributed, being February the month with the maximum frequency of avalanches recorded.

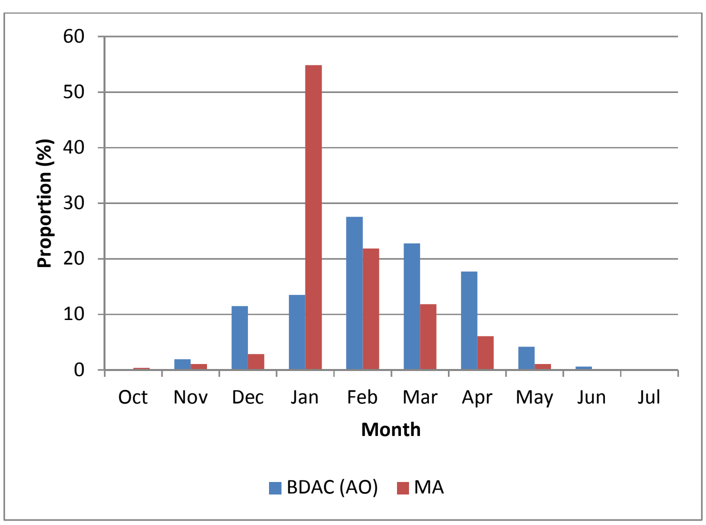

Figure 5. Frequency of Major Avalanches (MA, n=279 out of 654) in relation to Avalanche Observation (AO) registered in the BDAC since 1971 (n=1644 out of 3052).

3.3 Data treatment

We worked with periods P3 (19 winters from 1995/96 to 2013/14) and P2+P3 (113 winters from 1900/01 to 2013/14), separately, taking into account the different resolution of the data. The common MA parameters available for both periods, useful for the goal of this work were the spatial distribution, the temporal distribution and the runout distance. Runout distance and date of occurrence data together with vegetation analysis were after used for frequency/intensity determination.

3.3.1 Common parameters: spatial, temporal distribution and runout distance

All the recorded events were georeferenced according to their X and Y coordinates.

Winter season was considered the time unit to work in P2+P3. This fact forced us to discard many events in P2 that were not possible to date at that resolution. However, in P3, most of the events were dated at MAE time resolution.

Runout distance is the most sensitive parameter, because accuracy is variable depending on the source of information. The runout distance considered was determined from the destructive effects of the avalanche. This is the only common parameter for both periods, P2 and P3. Actually, what we compared is the minimum extent of the avalanche (Corona et al., 2012) as explained before. It should be noted that the range of uncertainty is significant, and it must be taken into account in the interpretation of results.

The extent of the different events for each avalanche path was mapped on the digital topographic and orthophoto bases 1:5000 of the ICGC, as shown in the example of Figure 6.

3.3.2 Frequency/Intensity

The relationship frequency/intensity of each event was obtained from the relative position of the different distances measured in the runout zone (Figure 6). In general it is expected that in a given avalanche path, as the average intensity increases downhill in the runout zone, the average frequency decreases (McClung, 2008). Thus, intensity is indirectly determined from the observed frequency. This is based on the principle that the farther the reach of the avalanche, the more intense it is, and the rarer is the avalanche, the more the probability of being observed decreases (Mears, 1992). The parameter used to find out this relationship was the relative runout distance between different events, in relation to the frequency of occurrence in each avalanche path.

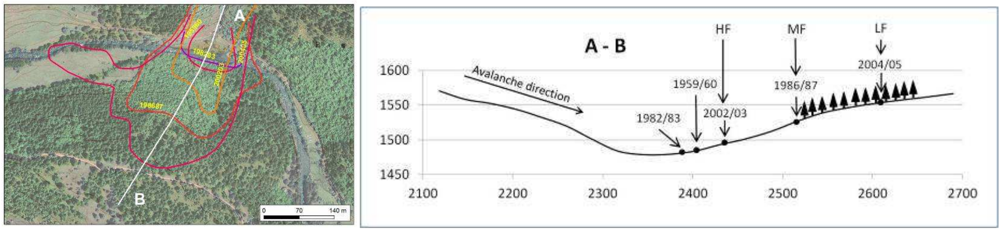

Figure 6. Example of runout distances reached by different avalanches in a given avalanche path, mapped (left) and plotted in a topographic profile (right). HF, MF and LF: high, medium and low frequency avalanche reaches.

The return period is the time interval in which the runout distance is achieved or exceeded in a given point. Frequency is the reciprocal of the return period. It is therefore possible, in principle, to map return periods in the runout zone corresponding to different distances downhill, for example, 1 year, 10 years, 100 years, corresponding to a mean annual probability of 1, 0.1 , 0.01. These distances increase in the runout zone at the same time that the return period increases (McClung and Schaerer, 2006). Given the lack of data generally everywhere, avalanche frequency can be estimated as an order of magnitude (Mears, 1992; Weir, 2002). Mears (1992) indicated that the return period (T) describes a range of time. According to the author, given this uncertainty, for an avalanche to which we assign a return period of 10 years based on our observations, the return period would be between 3 and 30 years, while a 100-year avalanche would have a T between 30 and 300 years. In any case, the range of uncertainty diminishes in relation to the number of events available for each avalanche path.

Based on the classification table of mountain hazards by Weir (2002), a classification of the avalanche frequency was defined for each avalanche path (Table 2). The error assigned to the frequency is indicated according to Mears (1992).

Table 2. Frequency classes established for the treated avalanches (based on Weir, 2002). Values in parentheses indicate the range of uncertainty.

Frequency classes	Return period (y)	Annual probability of occurrence
Very high (VHF)	5 (1-10)	0.2 (1-0.1)
High (HF)	10 (5-30)	0.1 (0.2-0.03)
Moderate (MF)	30 (10-100)	0.03 (0.1-0.01)
Low (LF)	100 (30-300)	0.01 (0.03-0.003)
Very low (VLF)	300 (>100)	<0.003 (<0.01)

To determine the frequency in the runout zone three criteria (absolute and relative) were considered: (i) number of times that events with similar runout distances were repeated in relation to the lapse of time between them (absolute), (ii) vegetation clues as a reference (absolute), and (iii) space/time relationship between runout distances of avalanches recorded in each avalanche path (relative).

Very high frequency avalanches were not considered MA according to the criteria used in this study. There are no cases in which these avalanches have affected forest. High frequency avalanches affect forest often, but not always. At least 20% of the high frequency avalanches recorded in forested paths, did not affect forest. This means that possibly the record of high frequency avalanches is not complete in P3 (we cannot guarantee a complete record if there is no evidence). On the contrary, we consider that the register of moderate to very low frequency avalanches is almost complete in P3 (figure 7). The long time interval between one avalanche and the next allows the forest to recover and, in the following episode, it will be affected. The same, but more pronounced, happens with low and very low frequency avalanches.

The number of MA in which the frequency could be determined in P1, P2 and P3 is shown in Figure 7. As it can be observed, the older is the period, the lower is the frequency of the registered MA. Time filters high frequency events, which are less destructive and therefore less perceived by the inhabitants, and only the most important MA reach us from written and oral sources.

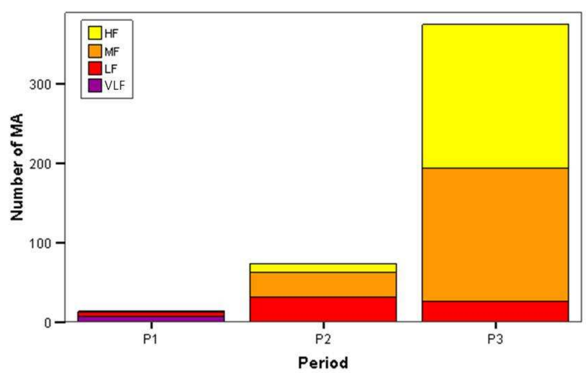

Figure 7. Number of Major Avalanches (MA) from which we could determine its frequency in P1, P2 and P3 time periods (n=633 out of 654). HF, MF, LF, VLF: high, moderate, low and very low frequency major avalanches.

In Figure 8 the distribution of the registered episodes in P3, number of MA registered per episode and its estimated frequency is displayed. The mean is 1.6 MAE per winter, but with a high variability (standard deviation equals 1.6), with some winters without MAE and winters with up to 5 MAE. Only 7 winters register more than 10 MA, and the largest episodes just exceeded 50 MA (22-23 January and 6-8 February 1996, 30-31 January 2003 and 24-25 January 2014). High frequency avalanches from 1995/96 episodes were probably underestimated because at that time, the surveillance service was at its initial stage and it was less efficient than nowadays.

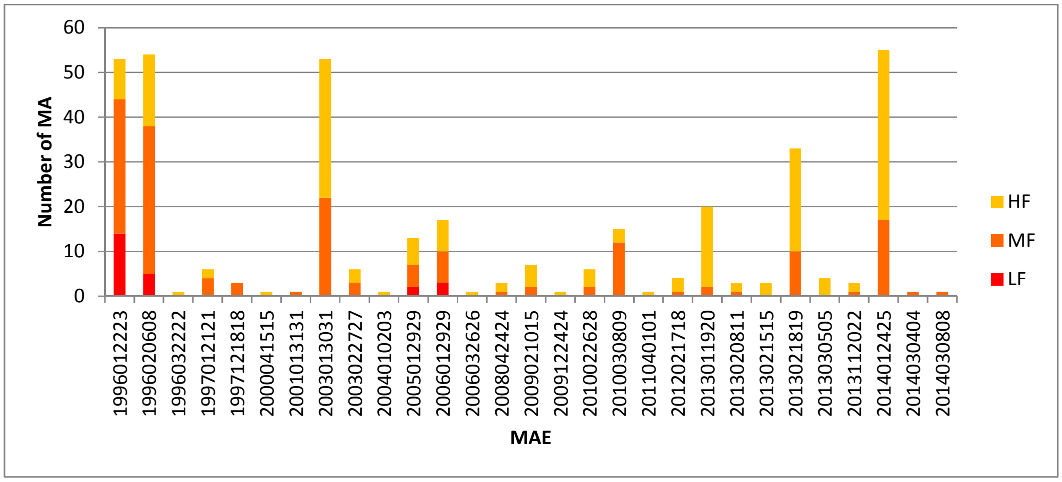

Figure 8. Frequency assigned to Major Avalanches (MA) per Major Avalanche Episode (MAE) in P3 period. Date of episodes has the format $YYYYMMD_1D_1D_2D_2$, where D_1D_1 is the first and D_2D_2 the last day of the episode. HF, MF, LF: high, moderate and low frequency.

In three of the registered MAE (6-8 February 1996; 30-31 January 2003; 24-25 January 2014), urban areas were attained by MA. In the first case a hostel was seriously damaged, in the second case a house was totally destroyed and another partially damaged, and in the third case, a touristic-apartments building was damaged at functional level. These three episodes are the ones which registered most avalanche occurrences. It is important to point out that all the damaged buildings were built after the seventies of the twentieth century in previously uninhabited areas.

The distribution of MA activity per winter and estimated frequencies in P3 (Figure 9) show how the lowest frequencies were registered during the first half of this period, being the second half more active owing to the number of major-avalanche winters and the frequency of MAE occurrences (Figure 10).

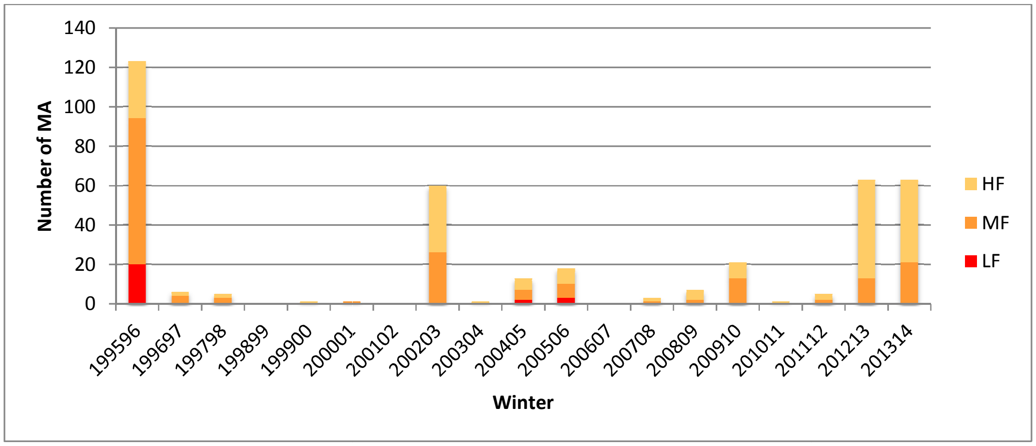

Figure 9. Frequency assigned to Major Avalanches (MA) per winter in P3 period. Date of winter has the format $Y_1Y_1Y_1Y_1Y_2Y_2$, where $Y_1Y_1Y_1Y_1$ is the year in which the winter season starts, and Y_2Y_2 identifies the consecutive year. HF, MF, LF: high, moderate and low frequency.

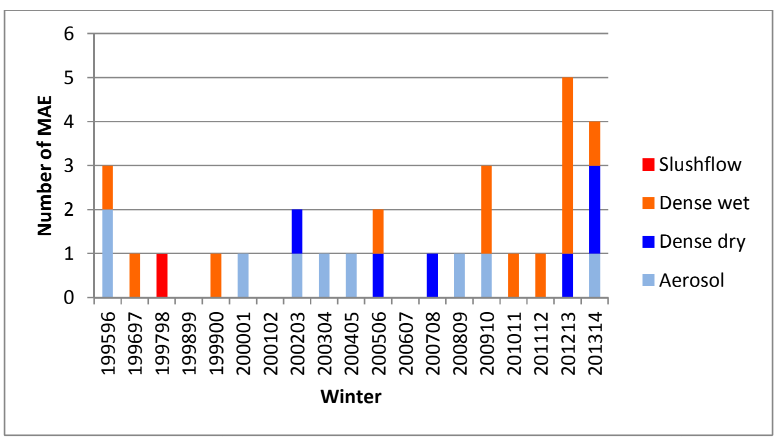

Figure 10. Number of Major Avalanche Episodes (MAE) per winter registered for P3, and observed avalanche dynamics (light blue: aerosol, dark blue: dense dry, orange: dense wet, red: slushflow). Date of winter has the format $Y_1Y_1Y_1Y_1Y_2Y_2$, where $Y_1Y_1Y_1Y_1$ is the year in which the winter season starts, and Y_2Y_2 the decade of the consecutive year..

4 Analysis and results

4.1 Analysis of the period P3 (1995/96-2013/14)

4.1.1 Temporal analysis

A primary objective of this study was to quantify the magnitude of the registered MAE. For such a purpose an index was conceived, similarly to Schweizer et al (1998) and Haegeli and McClung (2003). In the case of these authors, they applied an index on a daily basis (Avalanche Activity Index, AAI), that is to get a value of the daily activity of avalanches. They based it on the avalanche size, according to the Canadian avalanche size scale (McClung and Schaerer, 2006). They used the sum of all observed avalanches considering a weight according to its size. In our case, since we only worked with MA, mostly sizes 3 and 4, we used the frequency to emphasize the exceptionality of the episode. Major avalanches were classified in 4 classes (from 2, high frequency, to 5, very low frequency) and a weight inversely proportional to the estimated frequency of each avalanche was assigned (0.1, 0.3, 1 and 3). Like that we gave prominence to the lower frequency avalanches, the most intense, and at the same time, the small weight of HF MA prevents significant deviations caused by the incompleteness of this frequency class. The obtained parameter was called Major Avalanche Activity Magnitude Index (MAAMI). The MAAMI quantifies the magnitude of a MA for a period of time. It can be applied to the time scale allowed by the data resolution, e. g., episode, month, winter. In P3 we could apply this index at MAE resolution following the expression 1.

$$MAAMIe = \left[\left(\frac{\mathrm{N_{HF}}e}{\max\,(\mathrm{N_{HF}}e)}\cdot 0{,}1\right) + \left(\frac{\mathrm{N_{MF}}e}{\max\,(\mathrm{N_{MF}}e)}\cdot 0{,}3\right) + \left(\frac{\mathrm{N_{LF}}e}{\max\,(\mathrm{N_{LF}}e)}\cdot 1\right) + \left(\frac{\mathrm{N_{VLF}}e}{\max\,(\mathrm{N_{VLF}}e)}\cdot 3\right)\right]\Big/4{,}4 \qquad \text{(expression 1)}$$

For each episode (*e*), avalanches were grouped according to their frequency and were divided by the maximum value registered in the dataset for standardization. $\mathrm{N_{HF}}e$ is the number of high frequency MA recorded in an episode *e*, and $\max(\mathrm{N_{HF}}e)$ is the maximum number of recorded high frequency MA in a MAE. The resulting value for each frequency class is multiplied by the weight assigned to it. The final value is divided by 4.4, to obtain a result between 0 and 1.

The MAAMI*e* is also an exceptionality index of the MAE for the analyzed period. The resulting values respond to a logarithmic scale. Following the same reasoning about the weight assigned to the exceptionality of an avalanche, values were classified as shown in table 3.

Table 3. MAAMI values classification.

MAAMI	
Classes	Numerical value

Low	<0.03
Moderate	0.03 – 0.1
High	0.1 – 0.3
Very high	>0.3

In P3 period (19 winters) the MAAMI*e* was calculated for the 29 recorded episodes (Figure 11). We obtained high values for January and February 1996 episodes, even though January could be considered to be very high. For 30-31 January 2003, 29 January 2005, 29 January 2006, 18-19 February 2013 and 24-25 January 2014, the MAAMI*e* values were moderate, and for the rest of MAE values were low.

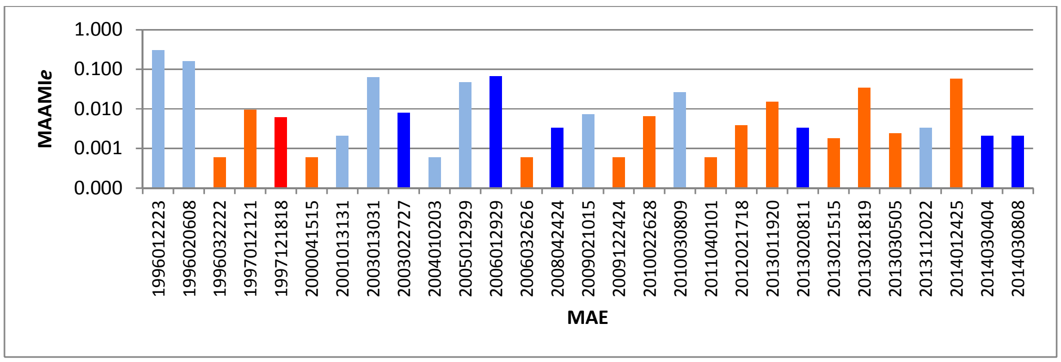

Figure 11. MAAMI*e* values obtained for P3, and observed avalanche dynamics (light blue: aerosol, dark blue: dense dry, orange: dense wet, red: slushflow) per Major Avalanche Episode (MAE). The scale of the ordinate axis is logarithmic. Date of episodes has the format $YYYYMMD_1D_1D_2D_2$, where D_1D_1 is the first and D_2D_2 the last day of the episode.

For each episode, the extent of the area deforested by avalanches was mapped and measured (Figure 12). This parameter is also an indicator of the exceptionality of the episode. We correlated the MAAMI*e* values with the deforested area values and we obtained a Pearson correlation coefficient of 0.96, which reinforces the validity of the MAAMI*e* as an indicator of MAE magnitude.

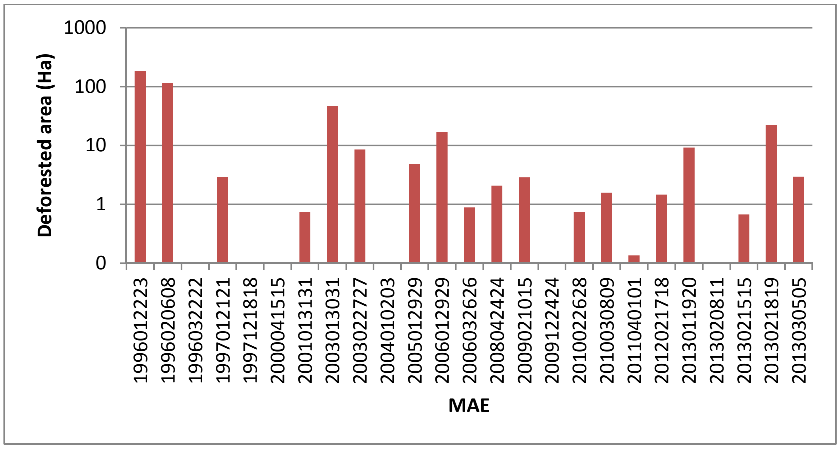

Figure 12. Deforested area per Major Avalanche Episode (MAE), for P3. The scale of the ordinate axis is logarithmic (2013/14 MAE deforested areas were not added to the dataset because the mapping process was not finished at the date of the publication of this work).

The obtained MAAMI*e* values were associated with each atmospheric circulation pattern defined by García-Sellés et al. (2009). In table 4 all registered episodes, observed dynamics per episode and corresponding MAAMI*e* values are listed.

Table 4. Registered Major Avalanche Episodes in P3 period and corresponding number of registered MA, observed dynamics, deforested area and MAAMI*e* values.

Episode	N	Estimated frequency (N)			Comp.	Observed dynamics	Deforested area (Ha)	MAAMI*e*
		H	M	L				
1996012223	53	9	30	14	S/SW	Dense dry and aerosol	187.7	0.295
1996020608	54	16	33	5	N/NW	Aerosol	114.3	0.159
1996032222	1	1	0	0	A	Dense wet	0.0	0.001
1997012121	6	2	4	0	E/SE2	Dense dry and dense wet	2.9	0.009
1997121818	3	0	3	0	E/SE1	Slushflow	0.0	0.006
2000041515	1	1	0	0	S/SW	Dense wet	0.0	0.001
2001013131	1	0	1	0	N/NW	Aerosol	0.7	0.002
2003013031	53	31	22	0	N/NW	Dense dry and aerosol	47.1	0.064
2003022727	6	3	3	0	E/SE1	Dense dry	8.6	0.008
2004010203	1	1	0	0	N/NW	Aerosol	0.0	0.001
2005012929	13	6	5	2	N/NW	Aerosol	4.9	0.046
2006012929	17	7	7	3	E/SE2	Dense dry and aerosol	16.7	0.067
2006032626	1	1	0	0	A	Dense wet	0.9	0.001
2008042424	3	2	1	0	S/SW	Dense dry	2.1	0.003
2009021015	7	5	2	0	N/NW	Dense dry and aerosol	2.9	0.007
2009122424	1	1	0	0	S/SW	Dense wet	0.0	0.001
2010022628	6	4	2	0	S/SW	Dense wet	0.7	0.007
2010030809	15	3	12	0	CL	Aerosol	1.6	0.027

2011040101	1	1	0	0	A	Dense wet	0.1	0.001
2012021718	4	3	1	0	N/NW	Dense wet	1.5	0.004
2013011920	20	18	2	0	S/SW	Dense wet and dense dry	9.2	0.015
2013020811	3	2	1	0	N/NW	Dense dry	0.0	0.003
2013021515	3	3	0	0	N/NW	Dense wet and dense dry	0.7	0.002
2013021819	33	23	10	0	E/SE1	Dense wet	22.3	0.034
2013030505	4	4	0	0	S/SW	Dense wet	3.0	0.002
2013112022	3	2	1	0	N/NW	Dense dry and aerosol	ND	0.003
2014012425	55	38	17	0	N/NW	Dense wet	ND	0.060
2014030404	1	0	1	0	N/NW	Dense dry	ND	0.002
2014030808	1	0	1	0	A	Dense dry/wet	ND	0.002

Major avalanche episodes with greatest MAAMI*e* values correspond to the pattern S/SW (with a high variability) as shown in Figure 13, and in the second place, to patterns E/SE2 and N/NW with less variability. The MAAMI*e* decreases considerably in CL and even more in E/SE1 MAE. It is merely testimonial in A MAE, since in these situations major avalanches have occurred sporadically.

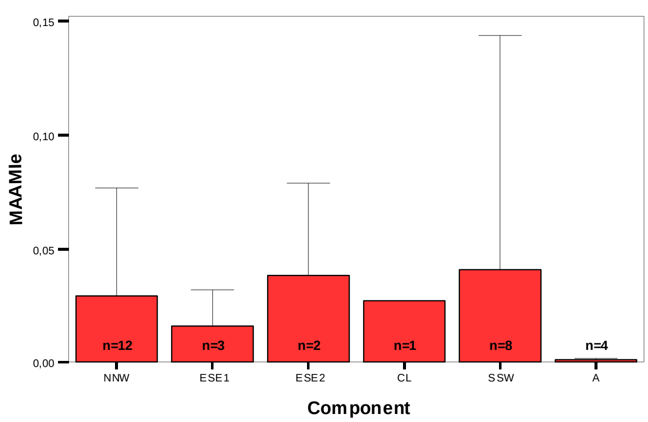

Figure 13. MAAMI*e* values (mean and standard deviation) related to their assigned atmospheric patterns.

In relation to the month of MAE occurrence (Figure 14), the highest values were obtained in January and February and, in decreasing order the following months until spring. November and December also registered low MAAMI*e* values. In those episodes in which a powder part was observed, the MAAMI*e* values were the highest, indicating that these are the most intense episodes. In contrast, the more dense and wet the avalanches, the lower the MAAMI*e* values (Figure 15).

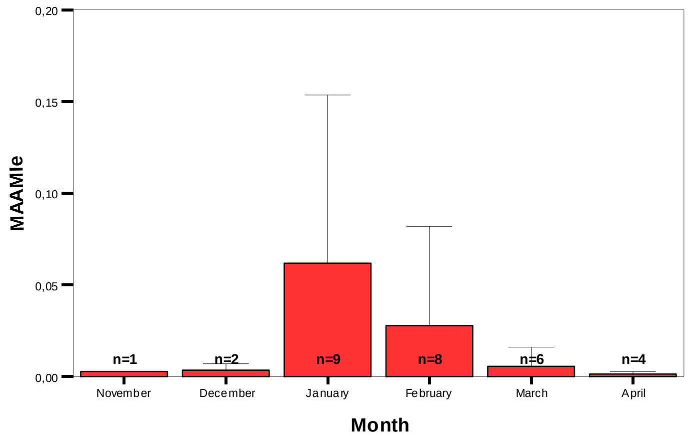

Figure 14. MAAMI*e* values (mean and standard deviation) related to the month of occurrence.

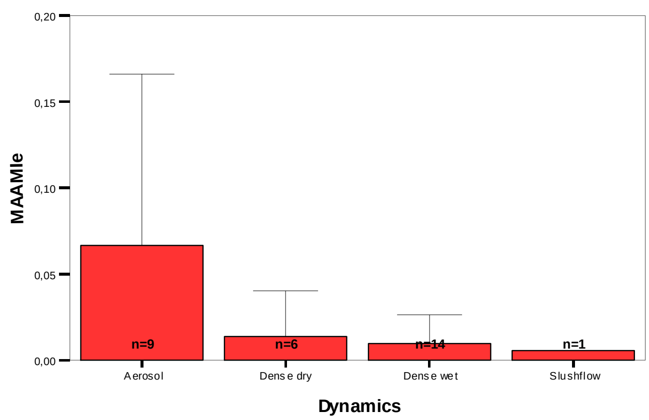

Figure 15. MAAMI*e* values (mean and standard deviation) of the episodes recorded in function of the observed dynamics.

However, these data must be interpreted with caution, since in some cases the standard deviation is greater than the average, indicating that we need to increase the sample size to confirm the results.

Considering winter season as the temporal unit for the same time period used for episode analysis (P3), we obtained the results shown in figure 16. From the 19 winters in P3 period, MAE were registered in 16 winters, being 1995/96 the most important Major Avalanche Winter (MAW), with very high MAAMI*w* values. On a second position, winters 2005/06, 2002/03, 2013/14, 2012/13 and 2004/05 (in decreasing order), registered moderate values, and the other winters registered low MAAMI*w* values, despite being significative in 2009/10.

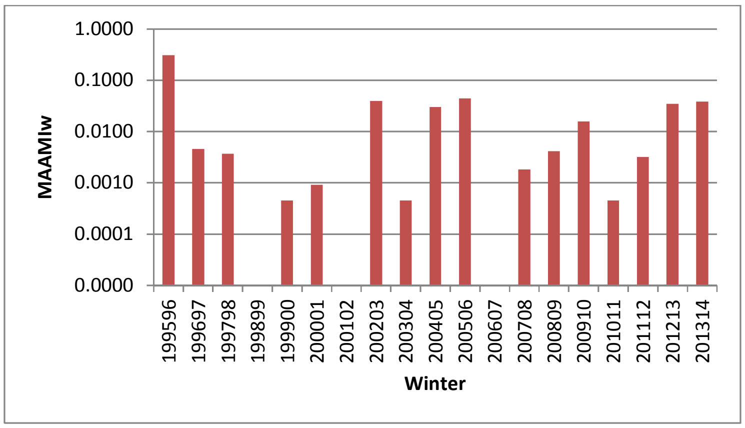

Figure 16. MAAMI*w* values obtained for the period P3. Date of winter has the format $Y_1Y_1Y_1Y_1Y_2Y_2$, where $Y_1Y_1Y_1Y_1$ is the year in which the winter season starts, and Y_2Y_2 identifies the consecutive year. The scale of the ordinate axis is logarithmic.

Note that when working considering winter season as the time period, the dataset is larger than when working with episodes, because we can add data dated at winter time resolution to the dataset. This is due to the inaccuracy of temporal data when the avalanche mapping has been done from vegetation clues in summer, in the field, or by photointerpretation.

We applied a logarithmic transformation to the MAAMI*w* values (log_MAAMI*w*) in order to obtain those for statistical treatment. We obtained a dataset with a good significance with the test of Shapiro-Wilk (p-value 0.32 for a α level 0.05), which means that the function fits to a normal distribution. Considering the data set (log_MAAMI*w*) a normal distribution, we obtained the estimated probability values (table 5). They indicate the annual estimated probability of occurrence of a log_MAAMI*w* value lower than a given value. For example, the annual estimated probability of occurrence of a winter with a MAAMI*w* value lower than 0.001 is 40% while the annual estimated probability of registering a winter with a MAAMI*w* lower than 0.3 is 97% (conversely, a MAAMI higher than 0.3 is 3%).

Table 5. Exceedance estimated probability of MAAMI*w* occurrence. The 95% confidence interval of the fitted distribution is [$1.54x10^{-4}$; $1.01x10^{-2}$].

MAAMI*w*		Estimated accum. probability
Class	Value	

Very low	<0.001	<0.40
Low	0.001 – 0.03	0.40 – 0.83
Moderate	0.03 – 0.1	0.83 – 0.93
High	0.1 – 0.3	0.93 – 0.97
Very high	>0.3	>0.97

As explained in section 3, urban areas were affected in 6-8 February 1996, 30-31 January 2003 and 24-25 January 2014 episodes, for which moderate to very high MAAMI*e* values were obtained. According to the results shown in table 5, the estimated annual probability of occurrence of a MAAMI*w* higher than 0.03 (moderate) which could affect urban areas, is 17%.

4.1.2 Spatial analysis

From the spatial distribution of the MA recorded in each MAE, the most likely affected area was reconstructed. Our reconstruction was based on the criterion that the behavior of air masses is strongly influenced by relief, causing 50 to 70% of mountain precipitation in winter (McClung and Schaerer, 2006). Orographic precipitation models include the assumption that precipitation is produced at a rate that is directly proportional to the rate at which the air is lifted (vertical component of wind velocity) over the mountains. The first mountain struck will usually induce the most precipitation and subsequent barriers receive less as the moisture supply in the air mass diminishes (McClung and Schaerer, 2006). This assumption is easily confirmed in the distribution of avalanches depending on the direction of the air mass that generated MAE.

In several occasions the occurrence of avalanches downwind from the direction of the air mass was observed. In other cases, the orographic lifting generated by the relief caused the triggering of avalanches on different aspects, possibly because the air mass was associated with weaker winds that did not condition the formation of overaccumulations downwind. On numerous occasions, the occurrence of major avalanches was not observed until reaching the highest elevations of the mountain range, although the air mass passed through avalanche prone areas but with lower elevations.

Taking these observations into account, we based the delimitation of the spatial extent of the different MAE according to the following criteria: (i) when the registered avalanche or avalanches were located in a valley open to the direction of the air mass, the whole valley was considered affected unless the extent of the episode could be clearly cut in a part of the valley, (ii) if the direction of the air mass was perpendicular to the valley, and last avalanches in the direction of the air mass were located upwind, the limit of the episode was mapped along the ridge of the valley, (iii) in the case that avalanches were registered on the leeward of the ridge, the border of the episode was mapped at the bottom of the valley. An example of how we mapped the spatial extent of MAE is shown in Figure 17 for winter 2002-2003.

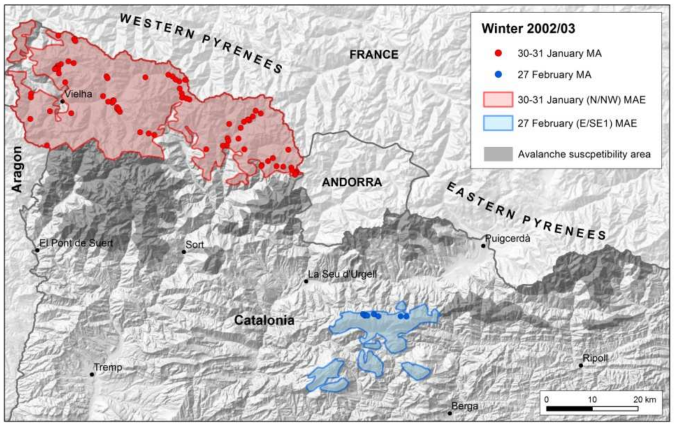

Figure 17. Map of the episodes inferred from the registered avalanches. Example from 2002/03 winter. Two episodes were reconstructed: 30-31 January (component N/NW) and 27 February (component E/SE1).

These arguments fitted very well for MAE which associated atmospheric pattern was the triggering factor of conditions leading to MA occurrence. Instead of this, in some episodes the spatial distribution of the recorded MA showed a typical configuration from other patterns. In these cases, the criteria explained in the previous paragraph had to be adapted. For instance, the 18-19 February 2013 MAE, classified as E/SE1, showed a typical N/NW pattern affected area (Figure 18), meaning that this MAE is the result of a preparation period and a later triggering one. During the first part, the unstable conditions are prepared, but it is in the second part that the episode is triggered. In fact, before 18-19 February 2013, two N/NW MAE occurred successively (8-11, and 15 February) with low MAAMI*e* values (few MA were registered). These which prepared the conditions for the following episode, a E/SE1, which tipically affects the easternmost PR and TF nivological regions, but in this case it affected only AR region, registering moderate MAAMI*e* values. This fact reinforces the idea that the study of MAE from a climatic point of view needs a wider temporal approach, considering previous atmospheric conditions (García et al., 2013), and at the same time, it supports the relationship between avalanche activity and a cumulative NAO index demonstrated by Keylock (2003).

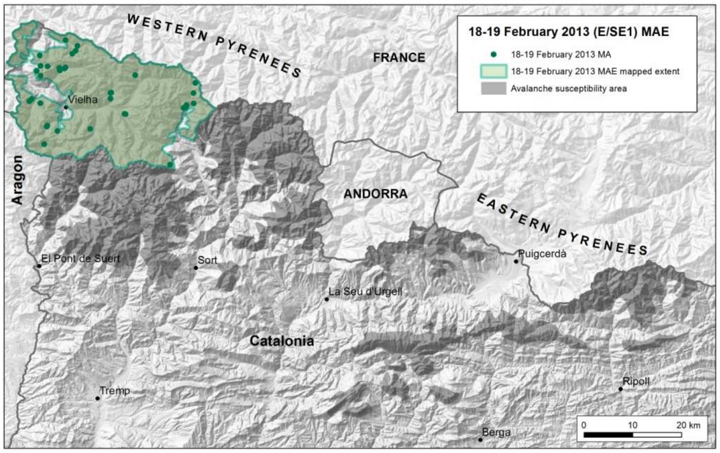

Figure 18. Map of 18-19 February 2013 episode inferred from the registered avalanches.

In order to better define the nivological regions (NR), the spatial extent of the different MAE was grouped according to their associated atmospheric patterns, described by García et al., 2009 (previously shown in table 1), and frequency and MAAMI*e* values were represented superimposed (Figures 19 to 25).

The N/NW configuration was the most frequent atmospheric pattern, with 10 recorded episodes. This pattern affects the north-western part of the study area more frequently than other parts (Figure 19, left). It is characterized by intense snowfalls, strong winds from north and northwest and very active snow drift processes. These episodes affected in a relative uniform way the AR region, and their frequency decreased towards the south, in PL and RF regions. The Eastern Pyrenees were only affected by one N/NW episode, except for the region TF and PP, the northern ones, which registered two other episodes close to their northern boundaries. In general these episodes showed high MAAMI*e* values (figure 19, right), but the sum of all gives a quite homogeneous result for all the regions with the highest values along the southern boundary of AR region. In the majority of cases, air masses coming from N and NW are the main drivers for N/NW episodes, but although AR region is the most affected, the strong weight of the MAAMI*e* obtained for the MAE of 6-8 February 1996, which origin was at least during the 22-23 January 1996 MAE, a S/SW pattern, gives a MA distribution more typically caused by a S/SW than by a N/NW MAE.

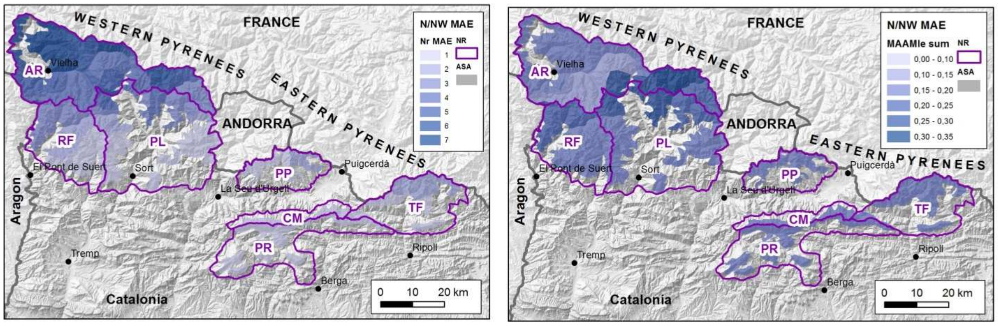

Figure 19. Spatial extent of the Major Avalanche Episodes (MAE) generated by N/NW atmospheric pattern. Frequency of MAE occurrence (left) and sum of the MAAMI*e* values of the superimposed events (right). NR: Nivological Regions; ASA: Avalanche susceptibility area.

Three E/SE1 episodes (Figure 20) were recorded. Two of them affected regions PR and CM with low MAAMI*e* values. One of these episodes corresponded to the slushflows occurrence in 1997/98 winter (Furdada et al., 1999), an exceptional phenomenon since avalanche activity is recorded in the Catalan Pyrenees, which affected a limited area. The third episode was registered in 18-19 February 2013 which as explained before, affected only the AR region although the atmospheric pattern associated to this episode was characterized by a southeast maritime flow at surface levels producing heavy precipitations in regions closest to the Mediterranean Sea. This MAE registered moderate values, the highest for a E/SE1 MAE.

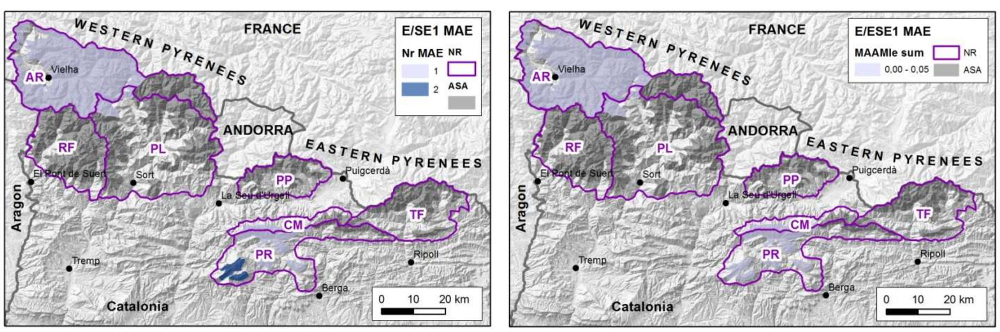

Figure 20. Spatial extent of the Major Avalanche Episodes (MAE) generated by E/SE1 atmospheric pattern. Frequency of MAE occurrence (left) and sum of the MAAMI*e* values of the superimposed events (right). NR: Nivological Regions; ASA: Avalanche susceptibility area.

The E/SE2 atmospheric pattern typically affects eastern and southern regions by worm and very humid Mediterranean flows on surface penetrating from east. Only two episodes were registered (Figure 21), but the affected areas do not overlap. The first episode affected RF region and the southern part of PL region, while the second one affected almost all the Eastern Pyrenees, excepting PP region. MAAMI*e* values were low for the first episode and moderate for the second. As a whole, the spatial extent of this pattern affected the southern part of the Pyrenees.

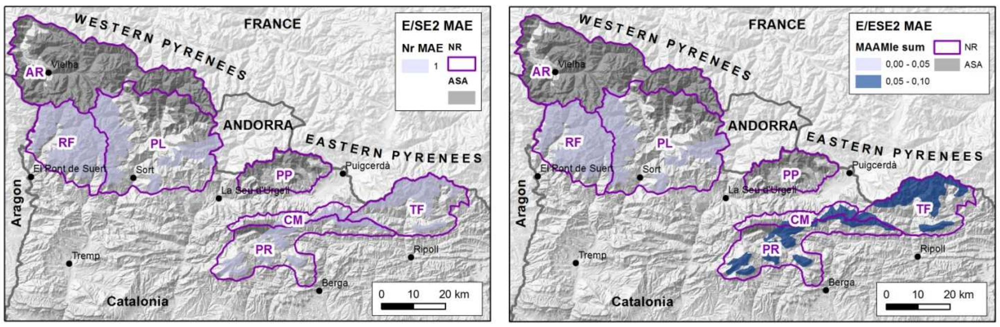

Figure 21. Spatial extent of the Major Avalanche Episodes (MAE) generated by E/SE2 atmospheric pattern. Frequency of MAE occurrence (left) and sum of the MAAMI*e* values of the superimposed events (right). NR: Nivological Regions; ASA: Avalanche susceptibility area.

There was only one CL atmospheric pattern episode registered (Figure 22), specifically the one of 8-9 March 2010, characterized by heavy snowfalls and northern strong winds, García et al (2009). It affected exclusively TF region with low/moderate MAAMI*e* values.

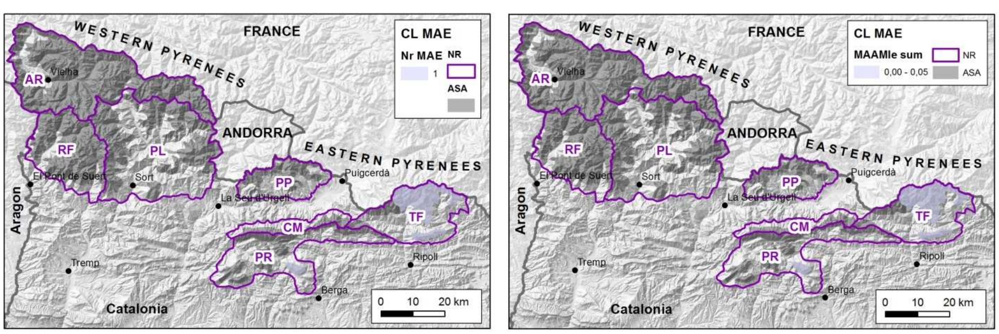

Figure 22. Spatial extent of the Major Avalanche Episodes (MAE) generated by CL atmospheric pattern. Frequency of MAE occurrence (left) and sum of the MAAMI*e* values of the superimposed events (right). NR: Nivological Regions; ASA: Avalanche susceptibility area.

S/SW episodes, typically characterized by south and southwestern wind flows carrying warm and humid air from the Atlantic and even the Mediterranean on lower levels over the Pyrenees, were the second pattern according to their frequency (7 MAE registered, Figure 23). They affected all NR but mainly the RF region and the western part of the PL region. Towards the east and the north, frequency decreased, affecting the rest of NR. In general, the recorded MAAMI*e* values were high for the southern regions (RF, PL, PP, CM, PR, TF), but low when they affected the northern one (AR). In fact, the highest MAAMI*e* value of the dataset is reached with the S/SW MAE of 22-23 January 1996, which is the only one considered a very high value. This value has an important weight in the results.

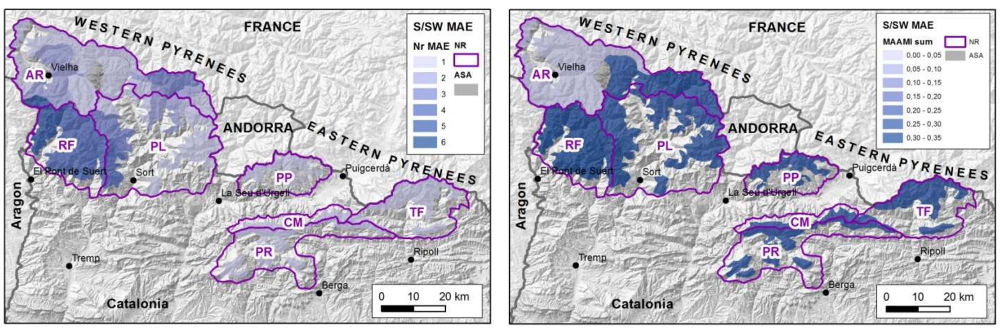

Figure 23. Spatial extent of the Major Avalanche Episodes (MAE) generated by S/SW atmospheric pattern. Frequency of MAE occurrence (left) and sum of the MAAMI*e* values of the superimposed events (right). NR: Nivological Regions; ASA: Avalanche susceptibility area.

Despite the fact that in A episodes the warm air mass can embrace a very large area of the Pyrenees, it only caused the triggering of avalanches occasionally. During P3 period, we identified three episodes (Figure 24), registering the lowest MAAMI*e* values.

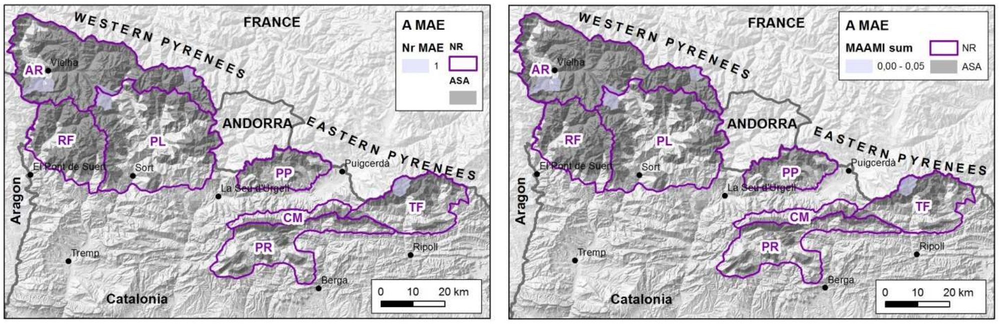

Figure 24. Spatial extent of the Major Avalanche Episodes (MAE) generated by A atmospheric pattern. Frequency of MAE occurrence (left) and sum of the MAAMI*e* values of the superimposed events (right). NR: Nivological Regions; ASA: Avalanche susceptibility area.

The superimposition of all the P3 MAE (29 episodes, Figure 25) showed a higher frequency in the AR, RF and western PL, in western Pyrenees, and TF, PR and CM in eastern Pyrenees. It is important to emphasize that PP region was only affected by 2 major episodes and therefore it is the region with the lowest MAE frequency. This is possibly due to its location, sheltered from the air masses that generate MAE, by the surrounding ranges. Instead of this, the southern regions registered higher MAAMIe values in comparison with the northern one AR (which drains towards the north), with the exception of its eastern arm (which drains towards the south). The highest values were recorded at the eastern arm of the AR region and northern RF and PL regions in the western part, and TF, CM and PF regions at the eastern part of the Pyrenees. Again, this result is dominated by the very high MAAMI*e* values from 1995/96 winter, which affected all the southern NR.

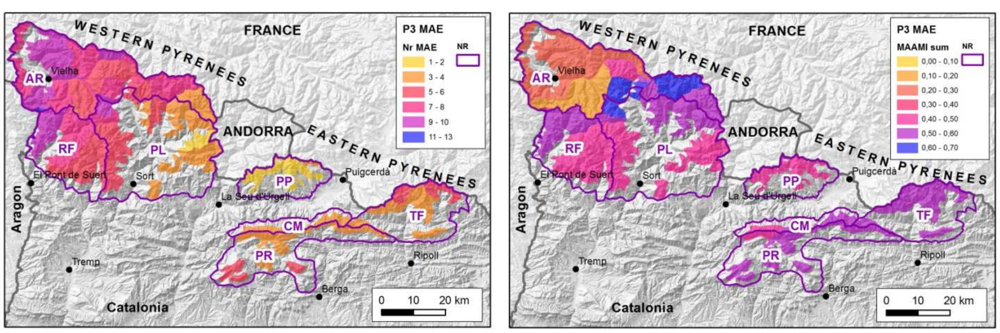

Figure 25. Map with the superimposition of all the registered Major Avalanche Episodes (MAE). Frequency of MAE occurrence (left) and sum of the MAAMI*e* values of the superimposed events (right). NR: Nivological Regions.

According to the spatial distribution of MAE and its corresponding MAAMI*e* values, the NR were redefined to better characterize the MAE spatial distribution. The new divisions were called Major Avalanche Nivological Regions (MANR). From west to east they are: GA (Garona), PN (Nord Pallaresa), RP (Ribagorçana-Pallaresa oest), PE (Pallaresa est), SN (Nord Segre), SL (Segre-Llobregat), TF (Ter-Freser) (Figure 26).

These regions can also be grouped according to the climatic influence, in oceanic influence regions, affected mainly by N/NW episodes (GA and PN); continental influence regions, affected mainly by S/SW episodes, but also N/NW (RP, PE and SN); and Mediterranean regions, affected by a high variety of atmospheric patterns (up to 5; SL and TF, figure 26).

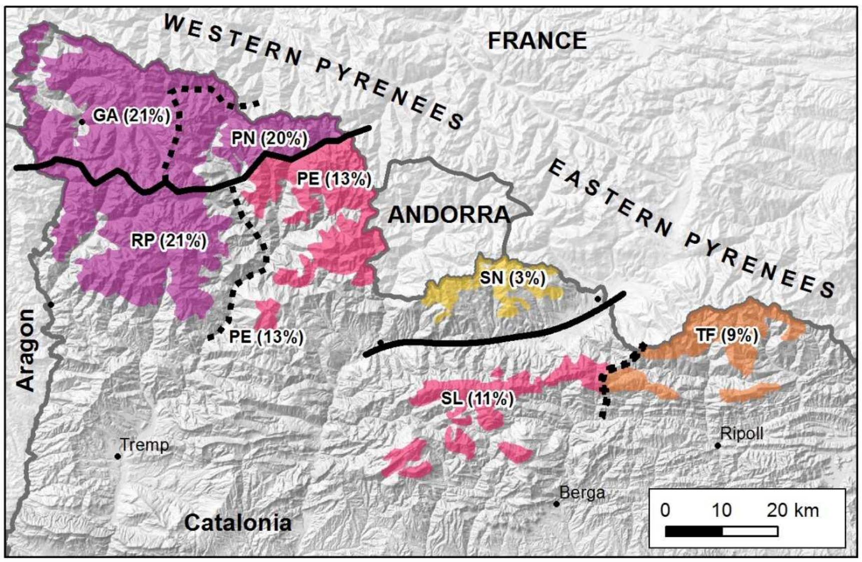

Figure 26. Major Avalanche Nivological Regions (MANR) defined from the frequency and spatial distribution of the registered Major Avalanche Episodes (MAE). Frequency of MAE occurrence in P3 is indicated in brackets. Black lines indicate main climatic divisions and dashed black lines, secondary divisions.

We divided AR NR into GA (chiefly Val d'Aran valley, western part of AR draining towards the north) and PN (eastern arm of the former AR, draining towards the south). The GA region is affected mainly by N/NW episodes (Table 6) and less frequently by S/SW and E/SE1 MAE. The PN region is a transitional MANR, affected by N/NW MAE as GA region, and less frequently by a more wider variety of MAE due to its open configuration towards the south. RP MANR is composed by the addition of the western part of PL NR to RF NR owing to their similar behavior. PE region is the remaining part of PL NR, similar to PN but less active. In regions RP and PE, N/NW episodes occur less frequently than in AR and PN. They are both affected also by E/SE2 and S/SW atmospheric patterns, but the main difference between them is the frequency of affectation by S/SW episodes. RP is the region most affected by S/SW episodes, which affect PE region less frequently. GA, PN and RP regions register the highest frequency of MAE occurrence. PE region is affected equally by N/NW episodes, and by southern component episodes, particularly E/SE2 and S/SW. N/NW episodes with high MAAMI*e* values are powerful enough to cross regions GA and PN. Episodes E/SE2 and S/SW can reach the top of the Noguera Pallaresa valley and adjacent valleys (PN region) due to its SW-NE direction, but they can't cross the French border ridges. SN is the region which presents the least MAE activity. It is affected only by the two main episodes of 1995/96 winter (S/SW and N/NW atmospheric patterns), and by one small N/NW MAE registered in 2013/14 winter. The low activity in this region may be due to the fact that it is located downwind of most air masses. Andorra mountains protect it from N/NW episodes and the Cadí range in the south protects it from E/SE1 and E/SE2 episodes mainly. SL region presents more frequent activity. This region and the TF region are the most varied regions in relation to the diverse origin of the MAE that affect them, mainly by southern episodes, but also by the N/NW episode of February 1996. In fact, SL is the only MANR that is affected by MAE generated by all described atmospheric patterns. It is logical, since the main orographic barrier oriented East-West (Serra del Cadí range), perpendicular to the direction of air masses coming from lower latitudes, dominates this region. Usually the main MA activity is observed on the north face of this range. The last region, TF, is affected by almost the same number of episodes than SL, but in this case it is not affected by E/SE1 episodes. Specifically, it is affected by 2 N/NW episodes, one E/SE2, one CL and one S/SW. It is the only area affected by CL atmospheric pattern.

From a climatological point of view, the occurrence of the several atmospheric patterns leading major avalanches is closely linked to low frequency atmospheric circulation patterns such as North Atlantic Oscillation (NAO) and Western Mediterranean Oscillation (WeMO) (García-Sellés et al., 2010). Two patterns are observed: the whole Catalan Pyrenees shows a good correlation between major avalanche activity and negative phase of NAO, but the oceanic domain has the particularity of concentrating major avalanche episodes in weak positive phases of NAO (N/NW). Even though for the period 1971–2008 NAO index shows a positive trend, there have been major avalanche situations linked to periods of highly negative phase of NAO (E/SE1, E/SE2, S/SW) (García-Sellés et al., 2010).

Table 6. Number of episodes identified in each MANR. Warm advection atmospheric pattern (A) was not considered because MAAMI*e* values associated to A episodes are very low. The intensity of the color indicates how often they have been repeated.

	MAE according to its associated atmospheric pattern					
MANR	N/NW	E/SE1	E/SE2	NE	S/SW	Total
GA	9	1			2	12 (21%)
PN	6	1	1		3	11 (20%)

RP	4		1		7	12 (21%)
PE	4		1		2	7 (13%)
SN	2				1	3 (5%)
SL	1	2	1	1	1	6 (11%)
TF	2		1	1	1	5 (9%)

4.2 Analysis of the period P2+P3 (1900/01-2013/14)

4.2.1 Temporal analysis

To characterize episodes recorded during P2+P3 period, we worked at winter season time resolution in order to adapt to P2 data limitations. Since the dataset was not complete, the calculation of the MAAMI was simplified considering the minimum frequency obtained from the entire MA registered per winter in each MANR, according to expression 2.

$$SMAAMI = \sum_{i=1}^{N} \frac{min(Fw_i)}{3 \cdot N} \qquad \text{(expression 2)}$$

This index was called Simplified Major Avalanche Activity Magnitude Index (SMAAMI), where min(Fw) corresponds to the lowest frequency of the MA recorded in one winter (w) for each of the 3 MANR (i stands for these regions). A low correlation MAAMIw-SMAAMI forced us to simplify the 7 MANR to 3, according to the main climatic divisions, for which the Pearson correlation was 0,75. The weight for the estimated frequencies (again, 0.1, 0.3, 1 and 3 from high to very low frequency MA) was assigned in order to highlight the less probable episodes. Divisor values correspond to the maximum value of the frequency (3) and maximum number of climatic regions (N=3) for standardization of the data.

The SMAAMI is a simplification of the MAAMI devised in case of less complete data series. It is based on the assumption that larger destructive avalanches are easier to remember than high frequency avalanches. Hence, the result has to be interpreted as an approximation. It highlights the maximum values registered in each region and therefore those episodes with low frequency MA and less extensive, against very extensive episodes but with high frequency MA.

In figure 27 the calculated SMAAMI values for P2+P3 are represented. Winter season 1995/96 shows the highest SMAAMI value, while the episodes of 1971/72, 1974/75, 1937/38, 2004/05, and 2005/06 show high SMAAMI values (in decreasing order), together with 14 other winters bordering the value 0.1. The remaining recorded MAE (25 winters) register moderate and low SMAAMI values.

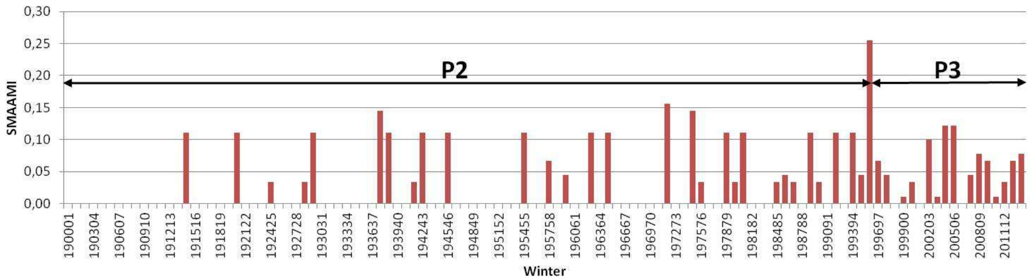

Figure 27. SMAAMI values obtained for P2+P3 period. Date of winter has the format $Y_1Y_1Y_1Y_1Y_2Y_2$, where $Y_1Y_1Y_1Y_1$ is the year in which the winter season starts, and Y_2Y_2 identifies the consecutive year.

P2+P3 provides a longer time period than P3 but more incomplete. For its analysis we adopted a compromise solution as was adopted by Keylock et al. (1999). We classified SMAAMI values into 6 classes in order to compare frequencies (Figure 28). Low values are better explained using P3 data, because the exhaustive surveillance task guaranties a good high frequency MAW record. On the other hand, we considered that in P2+P3 high SMAAMI values were more reliable because instead of being an incomplete data set, highest MAW should be those which would have been preserved through oral sources. For this reason, class 5 was assumed to contain the most realistic frequencies for both datasets. From this class to the lower ones, the distribution was scaled according to P3 distribution. Of course this is an approximation in order to reduce the lack of data in P2 and this weakness has to be taken into account when interpreting the results.

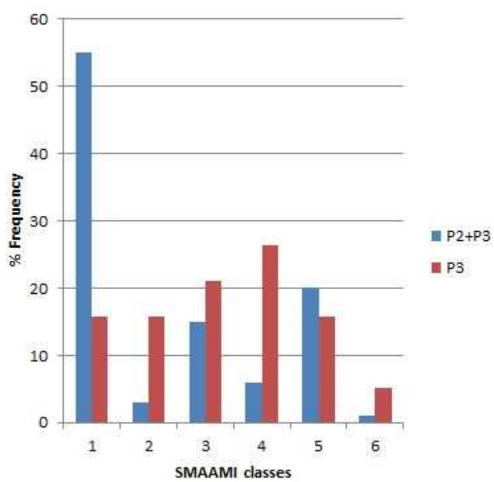

Figure 28. Relative frequency of SMAAMI classes for P2+P3 and P3 separately.

The statistical analysis of the resulting dataset provided good significance with the K-S test fitting to a Poisson distribution (p-value 0.28 for a α level 0.05). We obtained the probability values (table 7). They indicate the annual estimated probability of occurrence of a SMAAMI value lower than a given value. For example, the annual probability of occurrence of a winter with a SMAAMI value lower than 0.03 is 39% while the annual probability of registering a winter with a SMAAMI higher than 0.2 is 4%.

Table 7. Exceedance probability of SMAAMI occurrence. The 95% confidence interval of the fitted distribution is [2.89; 3.38].

SMAAMI		Estimated accum. probability
class	**value**	
1	<0.01	<0.18
2	0.01-0.03	0.18-0.39
3	0.03-0.06	0.39-0.62
4	0.06-0.1	0.62-0.79
5	0.1-0.2	0.79-0.90
6	>0.2	>0.96

Comparing the MAAMI*w* annual probability estimates (table 5) with those of SMAAMI (table 7), as could be expected, according to the different distribution function to which each dataset was fitted, values are significantly different. MAAMI*w* values are more than a 50 % higher for moderate values, decreasing to less than 10% for high values. It clearly indicates that although there is a high correlation between MAAMI*w* and SMAAMI, data shows a different MAE occurrence. This difference could be due to (i) the incompleteness of the P2 series, and (ii) the short period of P3 series.

4.2.2 Spatial analysis

Given the lack of information in P2, it was not possible to reach the same level of accuracy for the data set P2+P3. In many cases, the period P2 only registers one MA per winter. In this case the value 1 was assigned to the MANR that at least recorded a MA per winter. The results (Figure 29) show how for P2+P3, GA is the region where MAW were registered more often, followed by RP, PN and TF. Regions PE and SL were affected in a similar way and finally SN was the less affected region. This result, although NR are different, is remarkably similar to the one obtained for García-Sellés et al (2007), analyzing 1939-2006 period.

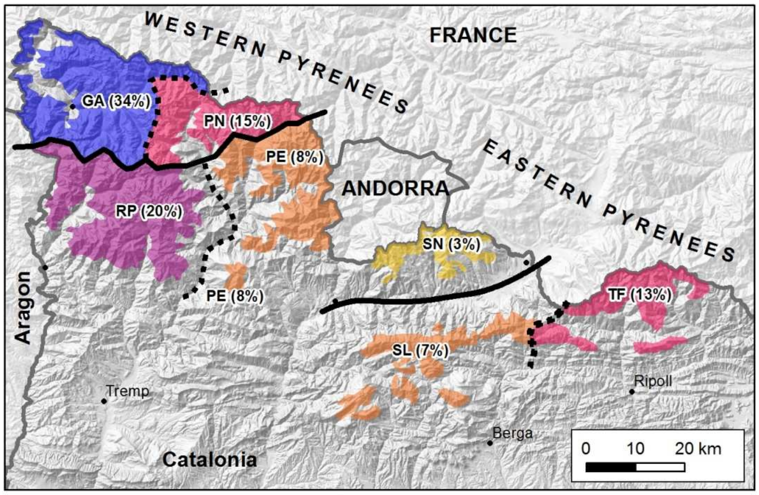

Figure 29. Frequency of Major Avalanche Winters (MAW) obtained for the period P2+P3 (values in brackets).

5 Discussion

This study provides a better understanding to the characterization of MAE over the Catalan Pyrenees. It was essential to have an exhaustive database with a detailed cartographic record of major avalanches. It allowed to reconstruct 29 major avalanche episodes from winters 1995/96 to 2013/14 (period P3) considering spatial distribution of MA and the atmospheric circulation patterns defined by García et al. (2009). On the one hand, it completes the information provided by these authors and on the other hand it incorporates new episodes. We did not follow, however, the same criterion to consider major avalanches. In the case of García et al. (2009) the criterion followed for considering MA was the size of the avalanche, while in the present work, the criterion was based on the destructiveness of the event. This makes the episodes considered not match in some cases.

The Major Avalanche Activity Magnitude Index (MAAMI) allowed quantifying the magnitude of avalanche episodes over the Pyrenees of Catalonia for the first time. This is a significant result because it enables quantifying and comparing the magnitude of avalanche episodes over a desired or possible time period. The SMAAMI index is a simplified resource when not much data are available and allows quantifying the magnitude of MAE at winter season resolution. It is based on the identification of the lower frequency MA recorded for each MANR per winter. It allowed us to reconstruct the series of the twentieth and early twenty-first centuries (P2+P3 periods), although it is not complete. The results show that the episodes of January and February 1996 are still the greatest known in the last 19 winters, and possibly two of the greatest in the last 100 years. This result is in accordance with that of Muntán et al. (2009), for the last 40 years. Other winters with high

SMAAMI values were 1971/72, 1974/75, 1937/38, 2004/05 and 2005/06 (in decreasing order). Although for the temporal periods P3 and P2+P3 we obtained a good correlation, probabilities obtained in both periods were significantly different. This result is probably due to the scattered dataset in P2 and the short temporal period in P3, in relation with the climatic variability typical of the studied area.

We also could characterize the MAE according to its associated atmospheric pattern in P3. It is important to note that southern atmospheric patterns (E/SE1, E/SE2, S/SW and A) are more varied and frequent that northern ones (N/NW, CL). The most surprising result was the high values of S/SW episodes. Registered S/SW episodes were the most powerful, while N/NW episodes were the most frequent. These results are dominated by 1995/96 episode, very infrequent according to the obtained probability, and for that reason results were probably biased. E/SE2 episodes recorded similar magnitude as N/NW ones, but they were much less frequent. Regarding the frequency with which the different atmospheric circulation patterns took place in P3, S/SW was more times observed than in the work of García et al. (2009), although component N/NW is the most registered, as was also indicated by these authors. The time window was different and the selection criteria of MAE too, and these facts could have had an influence on the results. Further analysis should clarify the reason for these differences. However, the spatial analysis results of this study match well with the results of García-Sellés et al. (2010), where major avalanche regions for the Catalan Pyrenees were grouped by applying clustering techniques. Attending to the major avalanche activity occurring at the same time (daily scale), regions were grouped in the three climatic domains: oceanic, continental and Mediterranean. On that study RP region was considered out of the oceanic domain as the shortest proximity distance by Ward method was shown to continental regions, but at the same time the isolated GA as oceanic domain showed a unique proximity relationship just with RP. That agrees with the fact that in this study, where recent winters are taken into account, RP, GA and PN show the first position in major avalanche activity, which could be expected from an oceanic region.

Regarding the risk, MAW which affected buildings reached MAAMI*w* values equal or higher than moderate. The estimated annual probability of occurrence of a MAW higher than moderate is 17%. All the affected buildings were touristic built after the seventies of the twentieth century. A better planning policy could avoid these accidents, too frequent under our point of view.

The spatial reconstruction of MAE from the registered MA showed, on the one hand, how MA distribution is controlled by snowpack-atmospheric evolution, and orography. In general, MA spatial distribution agrees with the low level air movement direction of the atmospheric pattern that triggers the MAE, following the valleys and diminishing its power when mountain ranges are arranged against its moving direction. Yet in 4 out of 29 MAE, MA distribution showed clear characteristics from other patterns. This was the case of 6-8 February 1996, a N/NW pattern with a S/SW configuration, the 19-20 January 2013, a S/SW pattern with a N/NW configuration, the 18-19 February 2013 (Figure 18), a E/SE1 pattern with a N/NW configuration, and 5 March 2013, a S/SW pattern with a N/NW configuration. This fact confirms that a MAE can not only be characterized by the atmospheric pattern that triggered it, but also by a previous preparatory period which should be considered (García-Sellés et al., 2013). This period, variable in time, prepares the conditions that can favour MA activity. These situations can also be identified indirectly using a cumulative NAO index (CNI), which exhibits a closer relationship to avalanche activity than the standard index (Keylock, 2013; García-Sellés et al., 2010). This preparatory process was not considered in the present work when classifying the MAE, only the atmospheric patterns triggering MAE were considered.

The analysis of MAE frequency, distribution and extent has enabled us to define 7 MANR different to the current NR, more adjusted to MAE extent, magnitude and frequency. These regions improve the characterization of MAE, but do not replace the existing NR, which are also used for high and very high-frequency events (not dealt with in this work), and which were defined for the communication of regional avalanche forecasting.

According to the climatic zoning defined by Garcia et al. (2007), in P3, MANR GA and PN would have greater oceanic influence. However GA region, 75% of the received episodes were N/NW, namely 12 (21 %). In contrast PN region was also affected (around 50%) by episodes S/SW, E/SE1 and E/SE2, adding more episodes to the N/NW ones (11, 20%). Eastward frequency decreases, from RP to SN regions, where in this last region the minimum affectation is recorded due to its location downwind of most components. This area has only been stricken by the MAE that affected almost all regions. Thus, MANR RP (21%), PE (13%) and SN (3 %), are located in the area of continental influence. It is an area with a strong gradient, where one of the most frequently affected and the less frequently affected regions (RP and SN) are located. In the eastern sector, MAE increase in frequency in SL and TF regions (11% and 9% respectively) due to the Mediterranean influence.

The results in P2+P3 also present some significant differences with the results obtained in P3 period (Figures 26 and 29). A surprising result was that the homogeneity of MAE frequency registered in GA, RP and PN regions when analyzing P3 (around 20% each one) showed a positive deviation towards GA and TF regions, while the continental climate regions were less frequently affected in P2+P3. These results are in accordance to those obtained by Garcia-Sellés et al (2007) for the period 1939-2006. This imbalance between P3 and P2+P3 periods is also identified when comparing the temporal sequence in both time periods. In our opinion it could be due to three factors: (i) the deviation caused by data obtained through inquiries in P2, which favours the collection of data from historically denser populated areas, (ii) the incompleteness of the

P2 series, and (iii) the climate variability typical of this area, which makes atmospheric circulation to have different patterns at multiannual resolution, in relation to the relatively short time period analyzed in P3. We believe that a longer dataset would allow checking these results.

In spite of the fact that our most complete dataset (P3) covers from 1995-96 to 2013-14, 19 winters, and this is a short time interval, some trends can be pointed out which could be linked to the recent climate change. The number of MAE has increased in the second half of this period and at the same time, wet MAE, which register high MAAMIe values (figures 10 and 11) are more frequent. We believe that the time interval is too short for obtaining solid conclusions, but the maintenance of the MA surveillance, and an effort to complete the MA catalogue in P2 could provide very interesting information in relation to possible trends and its connection with climate change, as the results obtained by Eckert et al. (2010a, 2010b, 2013), or Laternser and Schneebeli (2002).

6 Conclusions

The work with cartographic information of avalanche data series allowed to better quantify and characterize major avalanche episodes in space and time during the last 19 winters and improved the treatment of the avalanche data series of the twentieth century in the Pyrenees.

The proposed index, MAAMI (and its simplified version SMAAMI), is intended to categorize the magnitude of major avalanche episodes or winters. The time scale depends on the resolution of available data. It was developed to facilitate comparing episodes, obtaining frequencies, and if the series are long enough, to find trends on major avalanche activity. MAAMI obtained values at major avalanche episode time resolution showed a very high correlation coefficient with its corresponding deforested area.

The obtained results confirm 1995/96 winter as the one which recorded the highest MAAMI and SMAAMI values from the early twentieth century to the present (P2, from 1900 to 1995, and P3, from 1995 to 2014). It also identified 1937/38, 1971/72, 1974/75, 2005/06 and 2004/05 as the winters with high SMAAMI values. Regarding the episodes (P3 period), 22-23 January and 6-8 February 1996 registered the highest MAAMI*e* values, followed by 30-31 January 2003, 29 January 2005, 29 January 2006, 18-19 February 2013 and 24-25 January 2014 episodes, with moderate values.

This index is useful for risk analysis in major avalanche events, both in forecasting and in crisis management. It can be used to define risk scenarios for civil protection purposes. Urban areas have been affected by avalanches with moderate to very high MAAMI*e* values, all of them by a N/NW atmospheric pattern. A better knowledge of these episodes would improve its temporal and spatial forecasting.

By employing this index, the former nivological regions were revised and new regions MANR were defined which better characterize major avalanche activity over the Catalan Pyrenees (from west to east: GA, PN, RP, PE, SN, SL and TF).

Among these regions, GA, PN and RP stand out for the highest number of major avalanche episodes, and RP and PN for the greatest MAAMIe values registered in P3. It is remarkable to note that region GA, despite being the area with the highest snow precipitation of the Catalan Pyrenees, registers a similar number of episodes than its neighbouring regions RP and PN. Concerning both periods P2 and P3, GA is the region registering the highest number of major avalanche episodes. In the future, a larger dataset should be used to check these results.

Regarding period P2 there was a significant number of recorded major avalanches that could not be dated at enough time resolution to be dealt with in this paper. In the future, intensive efforts will be required to rebuild this part of the series and improve our knowledge. The completion of P2 would give more consistency to the dataset and would allow the use of more advanced data analysis methods such as those used by Eckert et al (2010), not applied in this work. We still can get more information, especially in the field by using dendrochronology. In the same way, the study of P1 (previous to 1900) should help us to better understand the situations that generate the lowest frequency avalanches, only recorded in this period, and be prepared for when they happen again.

Acknowledgements: The authors are grateful to the following institutions: Conselh Generau d'Aran, FGC-Vall de Núria, Cos d'Agents Rurals, Consell Cultural de les Valls d'Àneu, Aran Culturau SCP, Registro Estatal de Accidentes por Alud, Associació per al Coneixement de la Neu i les Allaus, Arxiu Izard-Llonch i Forrellad. The authors are also grateful to the editor Nicolas Eckert and the two anonymous referees for their suggestions which substantially improved the manuscript.

7 References

Ancey, C. (2006). Dinamique des avalanches. Presses polythechniques universitaires romandes (Lausanne, Suisse) & Cemagref (Antony, France). 338 pp.

Carreras, J., Carrillo, E., Masalles, R., Ninot, J., Soriano, I., Vigo, J., 1996. Delimitation of the supra-forest zones in the Catalan Pyrenees. Bull. Soc. Linn. Provence 47, 27–36

Corona, C., Lopez, J., Stoffel, M., Bonnefoy, M., Richard, D., Astrade, L., Berger, F. (2012). How much of the real avalanche activity can be captured with tree rings? An evaluation of classic dendrogeomorphic approaches and comparison with historical archives. Cold Regions Science and Technology 74, 31-42, 21.

Barbolini, M., Keylock, C. J. (2002). A new method for avalanche hazard mapping using a combination of statistical and deterministic models. Natural Hazards and Earth System Sciences (2002) 2: 239-245.

Birkeland, K. W., Mock, C. J., Shinker, J. J. (2001). Avalanche extremes and atmospheric circulation patterns. Annals of Glaciology; 32:135-140.

Eckert, N., Parent, E., Belanger, L., Garcia, S. (2007). Hierarchical modeling for spatial analysis of the number of avalanche occurrences at the scale of the township. Cold Regions Science and Technology 50. 97-112.

Eckert N. (2009). Assessing the impact of climate change on snow avalanche activity in France over the last 60 winters using hierarchical Bayesian spatio-temporal change point models. Proceedings of the 18th World IMACS/MODSIM Congress, Cairns, Australia 13-17 July 2009. Pp 2604-2610.

Eckert, N., Baya, H., Deschartes, M. (2010a). Assessing the response of snow avalanche runout altitudes to climate fluctuations using hierarchical modeling: application to 61 winters of data in France. Journal of Climate 23, 3157-3180.

Eckert, N., Parent, E., Kies, R., Baya, H. (2010b). A spatio-temporal modelling framework for assessing the fluctuations of avalanche occurrence resulting from climate change: application to 60 years of data in the northern French Alps. Climatic Change 101: 515-553.

Eckert, N., Gaume, J., Castebrunet, H (2011). Usign spatial and spatial-extreme statistics to characterize snow avalanche cycles. Procedia environmental Sciences 7, 224-229.

Eckert, N., Keylock, C. J., Castebrunet, H., Lavigne. A., Naaim, M. (2013). Temporal trends in avalanche activity in the French Alps and subregions: from occurrences and runout altitudes to unsteady return periods. Journal of Glaciology. Vol. 59, No 213, 93-114.

Esteban, P., Jones, P.D., Martín-Vide, J., Mases, M., 2005. Atmospheric circulation patterns related to heavy snowfall days in Andorra, Pyrenees. International Journal of Climatology 25, 319–329.

Field Code Changed

Fitzharris, B.B.; Schaerer, P. A. (1980). Frequency of major avalanche winters. Journal of Glaciology, 26, (94), 43.

Furdada, G., Vilaplana, J. M., Bosch, X., Martínez, P. (1990). Supplying the Catalan Pyrenees (Spain) with a public avalanche warning system. Proceedings of the ISSW-1990 (Montana, USA): 119-129.

Furdada, G.; Martínez, P.; Oller, P.; Vilaplana, J.M. 1999. Slushflows at El Port del Comte, northeast Spain. Journal of Glaciology 45 (151), 555-558.

García-Sellés, C., Gavaldà, J., Martí, G., Martínez, P., Oller, P. (1996). Guia d'utilització del butlletí de perill d'allaus. 40 pp.

García-Sellés, C., Martí, G., García, A., Muntán, E., Oller, P., Esteban, P., (2007). Weather and snowpack conditions of major avalanches in the Eastern Pyrenees. Proceedings of the Alpine&Snow Workshop: Forschungsbericht, 53, 49–56.

García, C., Martí, G., Oller, P., Moner, I., Gavaldà., J., Martínez, P., Peña, J. C. (2009). Major avalanches occurrence at regional scale and related atmospheric circulation patterns in the Eastern Pyrenees. Cold Regions Science and Technology 59, 106-118.

García-Sellés, C., Peña, J.C., Martí, G., Oller, P., Martínez, P. (2010). WeMOi and NAOi influence on major avalanche activity in the Eastern Pyrenees. Cold Regions Science and Technology 64, 137-145.

García-Sellés, C., Manguán, S., Martí, G., Oller, P., Martínez, P. (2013). Combined temperature – precipitation winter modes and major avalanche activity in the Eastern Pyrenees. Proceedings of the ISSW 2013 (Grenoble – Chamonix Montblanc): 1264-1268.

Germain, D., Filion, L., Hétu, B. (2009). Snow avalanches regime and climatic conditions in the Chic-Choc Range, eastern Canada. Climatic Change 92: 141-167.

Haegeli, P., and McClung, D.M. (2003). Avalanche characteristics of a transitional snow climate - Columbia Mountains, British Columbia, Canada. Cold Regions Science and Technology, 37, 255-276.

Höller, P. (2009). Avalanche cycles in Austria: an analysis of the major events in the last 50 years. Nat Hazards 48:399-424.

Keylock, C. J., McClung, D. M., Magnússon, M. M. (1999). Avalanche risk mapping by simulation. Journal of Glaciology, Vol. 45, 150: 303-314.

Keylock, C. J. (2003). The North Atlantic Oscillation and snow avalanching in Iceland, Geographical Research Letters, Vol 30, Nº 5, 1254. 58-1, 58-4.

Laternser, M., Schneebeli, M. (2002). Temporal trend and spatial distribution of avanche activity during the last 50 years in switzerland. Natural Hazards 27: 201-230.

Lied, K. and Bakkehoy, S. (1980). Empirical calculations of snow-avalanche run-out distance based on topographic parameters. Journal of Glaciology, 26, (94): 165-177.

Martínez, P., Oller, P. (2004). Els accidents per allaus al Pirineu de Catalunya. Actes de la I Jornada Tècnica de Neu i Allaus. Barcelona, 16 de juny de 2004. Pp: 32-35.

Mears, A.I. (1992) Snow-avalanche hazard analysis for land use planning and engineering. Colorado Geological Survey, Denver. 55 pp.

McClung, D.M. (2008). Risk-based Land-Use planning in snow avalanche terrain. In: J. Locat, D. Perret, D. Turmel, D. Demers et S. Leroueil, (2008). Comptes rendus de la 4e Conférence canadienne sur les géorisques: des causes à la gestion. Proceedings of the 4th Canadian Conference on Geohazards : From Causes to Management. Presse de l'Université Laval, Québec, 594 p.

McClung, D.M., Schaerer, P. (2006). The Avalanche Handbook (3rd edition). The Mountaineers Books. Seattle. 342 pp.

Muntán, E., Andreu, L., Oller, P., Gutiérrez, E., and Martínez, P. (2004). Dendrochronological study of the avalanche path Canal del Roc Roig, First results of the ALUDEX project in the Pyrenees, Ann. Glaciol., 38, 173–179.

Muntán, E., García-Sellés, C., Oller, P., Marti, G., Garcia, A., Gutierrez, E., 2009. Reconstructing snow avalanches in the Southeastern Pyrenees. Natural Hazards and Earth System Science 9, 1599–1612.

Oller, P.; Marturià, J.; González, J.C.; Escriu, J.; Martínez, P (2005): El servidor de datos de aludes de Cataluña, una herramienta de ayuda a la planificación territorial. In proceedings of: VI Simposio Nacional sobre Taludes y Laderas Inestables. Valencia, 21-24 de Junio de 2005. E. P. 905-916.

Oller, P., Muntán, E., Marturià, J., García-Sellés, C., García, A., Martínez, P. (2006). The avalanche data in the Catalan Pyrenees. 20 years of avalanche mapping. Proceedings of the 2006 International Snow Science Workshop, Telluride, Colorado. Pp 305-313.

Rodés, P., Miranda, C. (2009). Aludes de nieve del pasado, anteriores al siglo XIX. Anales de Mediciona y Socorro en Montaña. 9: 8-14.

Schaerer, P. (1986). Winter weather. Weather patterns for major avalanches. The Avalanche Review, Vol. 4, No. 3.

Schneeneli, M., Laternser, M., Amman, W. (1997). Destructive Snow Avalanches and climate change in the Swiss Alps. Eclogae geol. Helv. 90, 457-461.

Schweizer, J., Jamieson, B., Skjonsberg, D. (1998). Avalanche forecasting for transportation corridor and backcountry in Glacier National Park (BC, Canada). Proceedings of the 25 years of snow avalanche research (Voss, Norway, 12-16 May 1998). E, Hestnes Ed. Norwegian Geotechnical Institute. 238-243.

SMC, UB, ICC, (1997). Atles Climàtic de Catalunya.

Stoffel, M., Butler, D. R., and Corona, C. (2013). Mass movements and tree rings: A guide to dendrogeomorphic field sampling and dating. Geomorphology, 200, 106-120.

Stokes, M. A., and Smiley, T. L.(1968). An introduction to tree-ring dating, University of Chicago Press.

Weir, P. (2002). Snow avalanche management in forested terrain. Res. Br., B.B. Min. For., Victoria, B.V. Land Manage. Handb. No. 55.

Figure(s)
Click here to download high resolution image

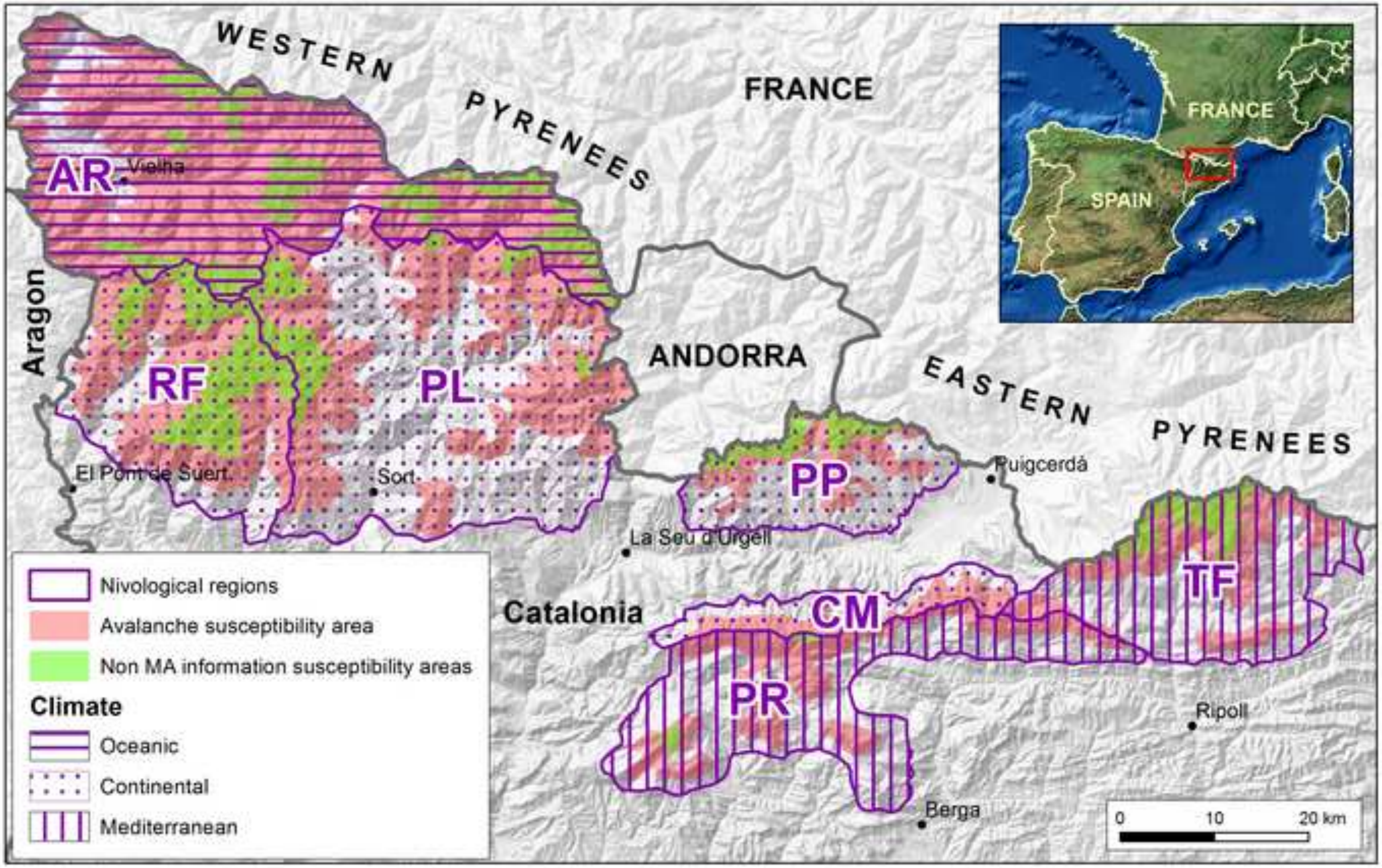

Figure(s)
Click here to download high resolution image

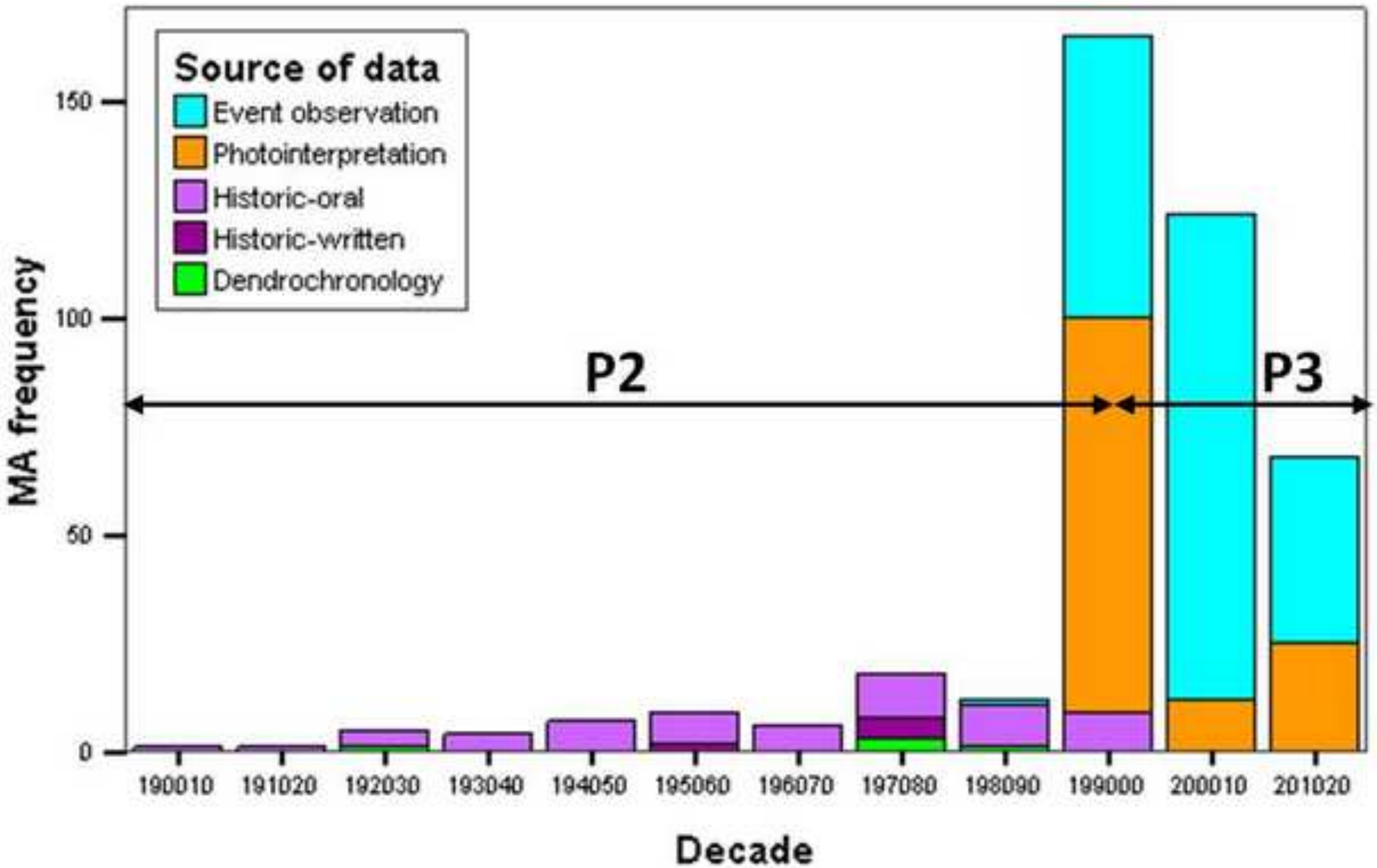

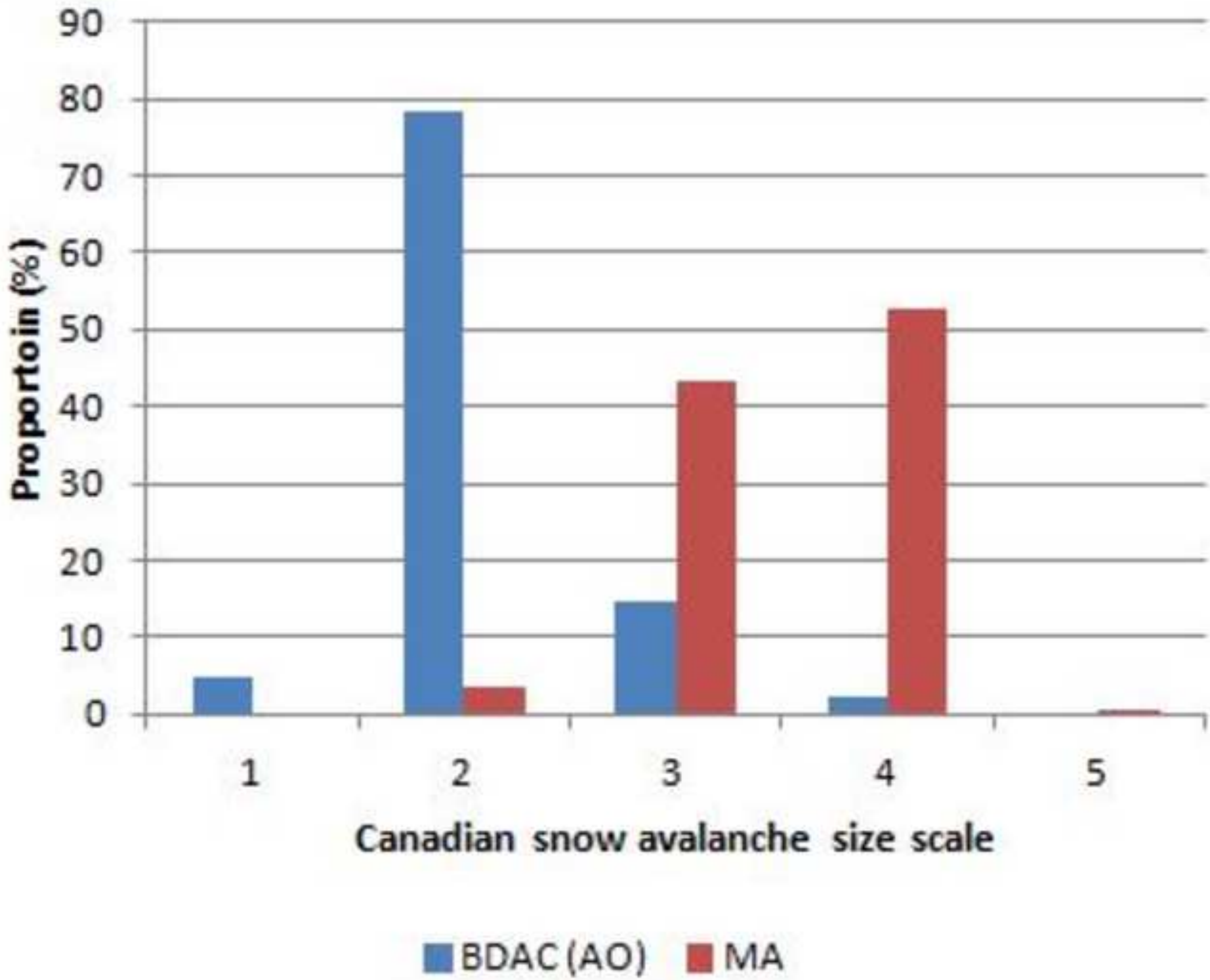
90
80
70
60
50
40
30
20
10
0
Proportoin (%)
1
2
3
4
5
Canadian snow avalanche size scale
BDAC (AO)
MA

Figure(s)

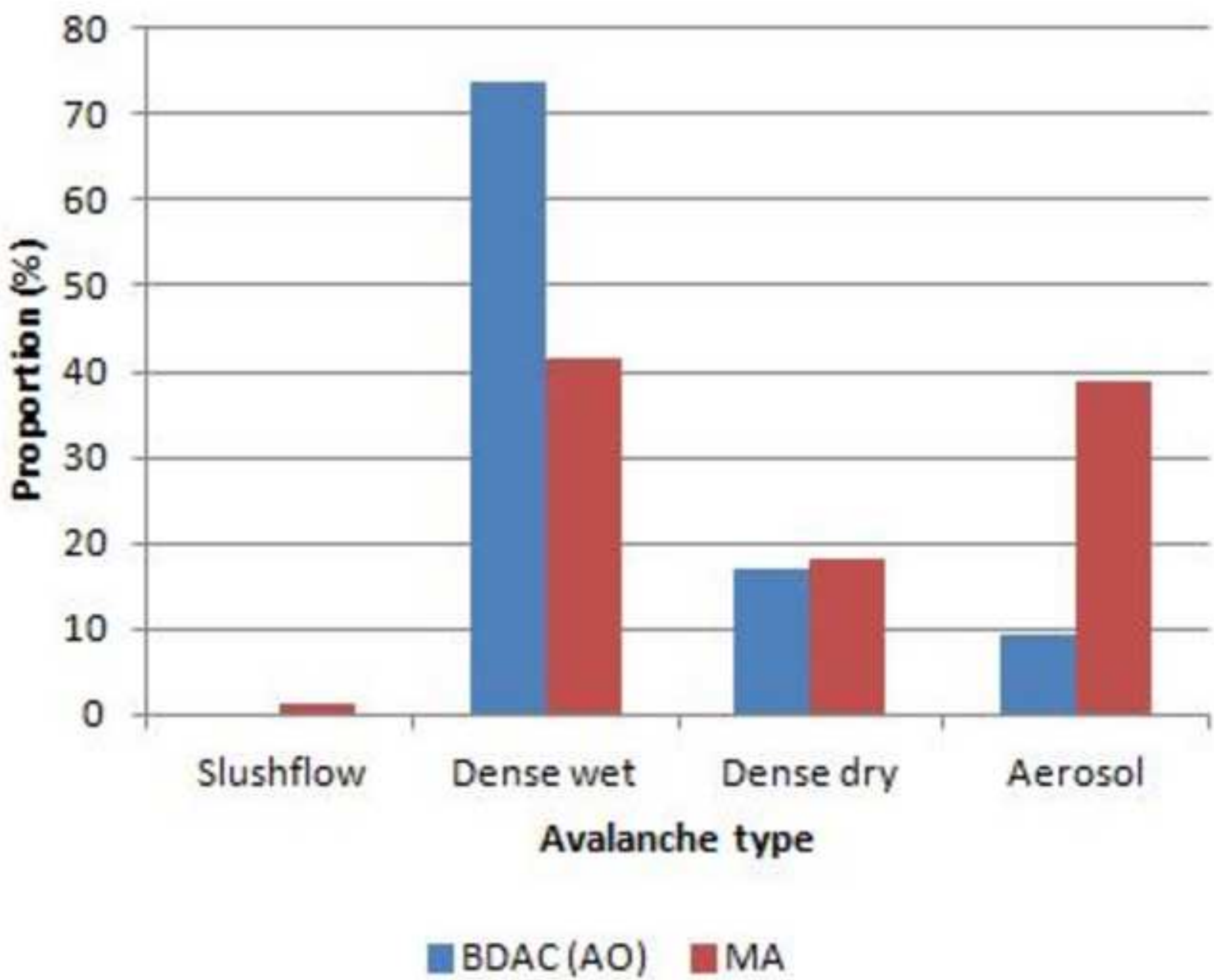
80
70
60
50
40
30
20
10
0
Proportion (%)
Slushflow
Dense wet
Dense dry
Aerosol
Avalanche type
BDAC (AO)
MA

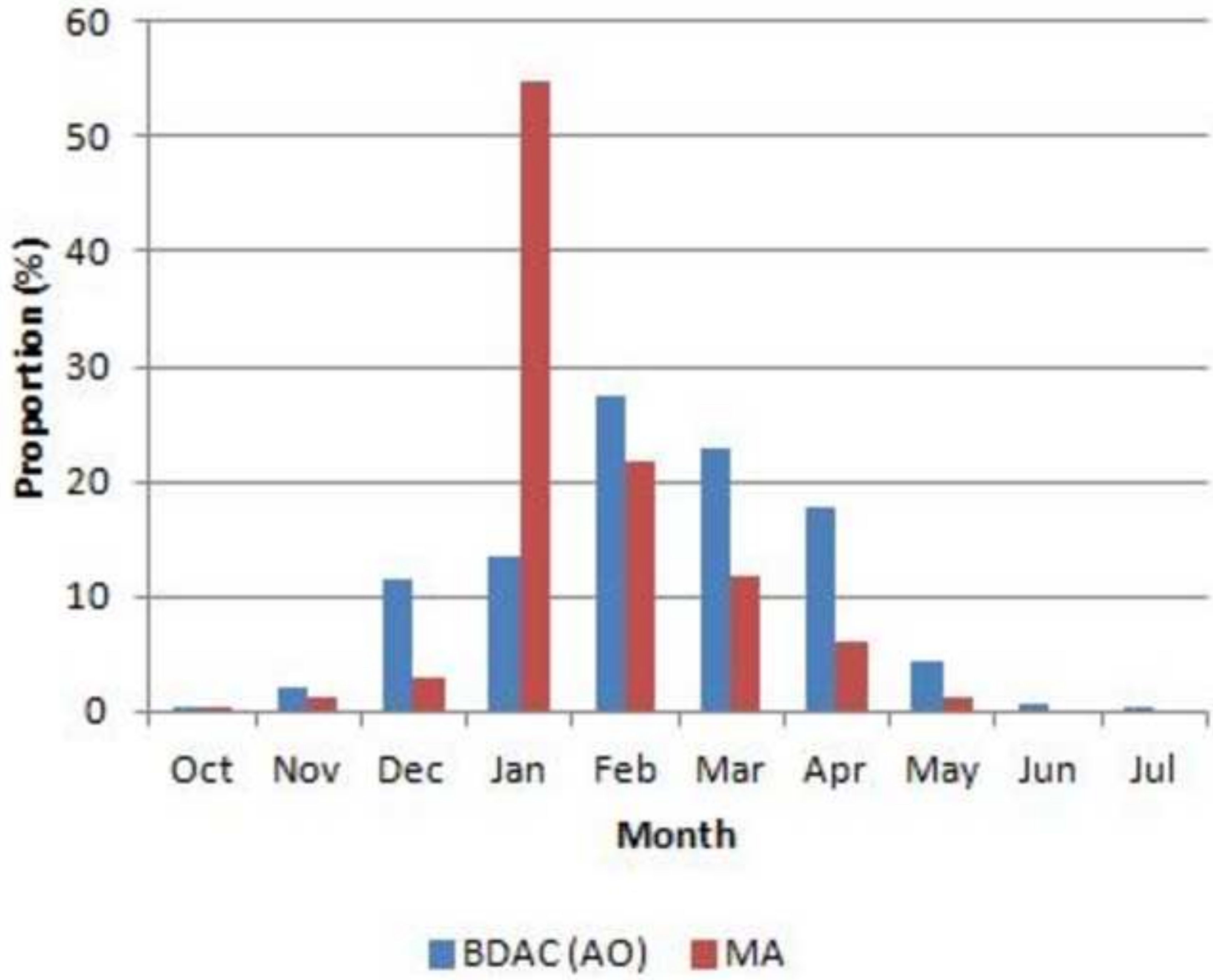
60
50
40
30
20
10
0
Proportion (%)
Oct
Nov
Dec
Jan
Feb
Mar
Apr
May
Jun
Jul
Month
BDAC (AO)
MA

Figure(s)
Click here to download high resolution image

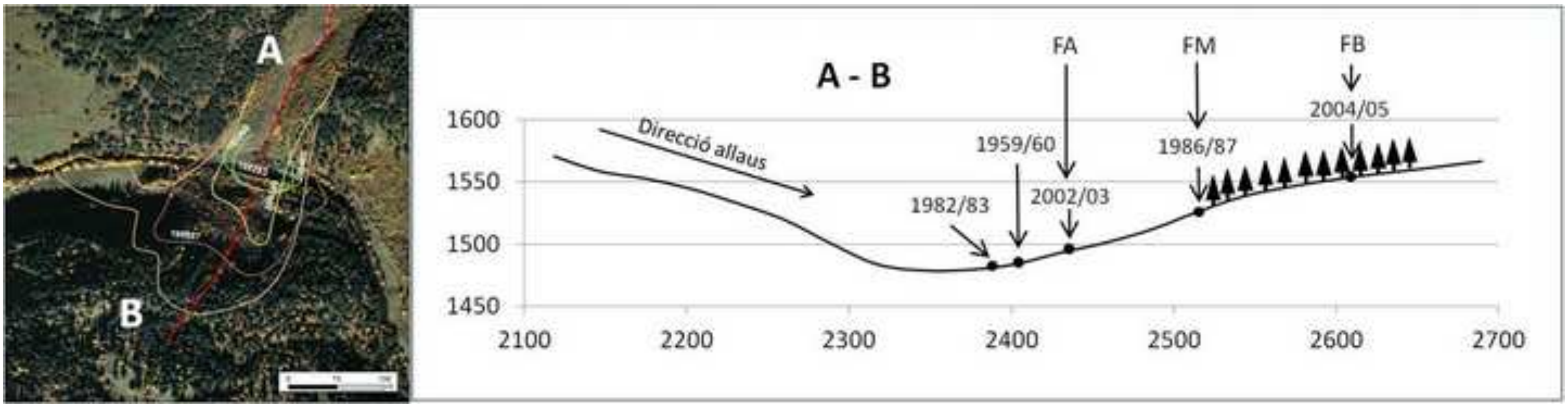

Figure(s)
Click here to download high resolution image

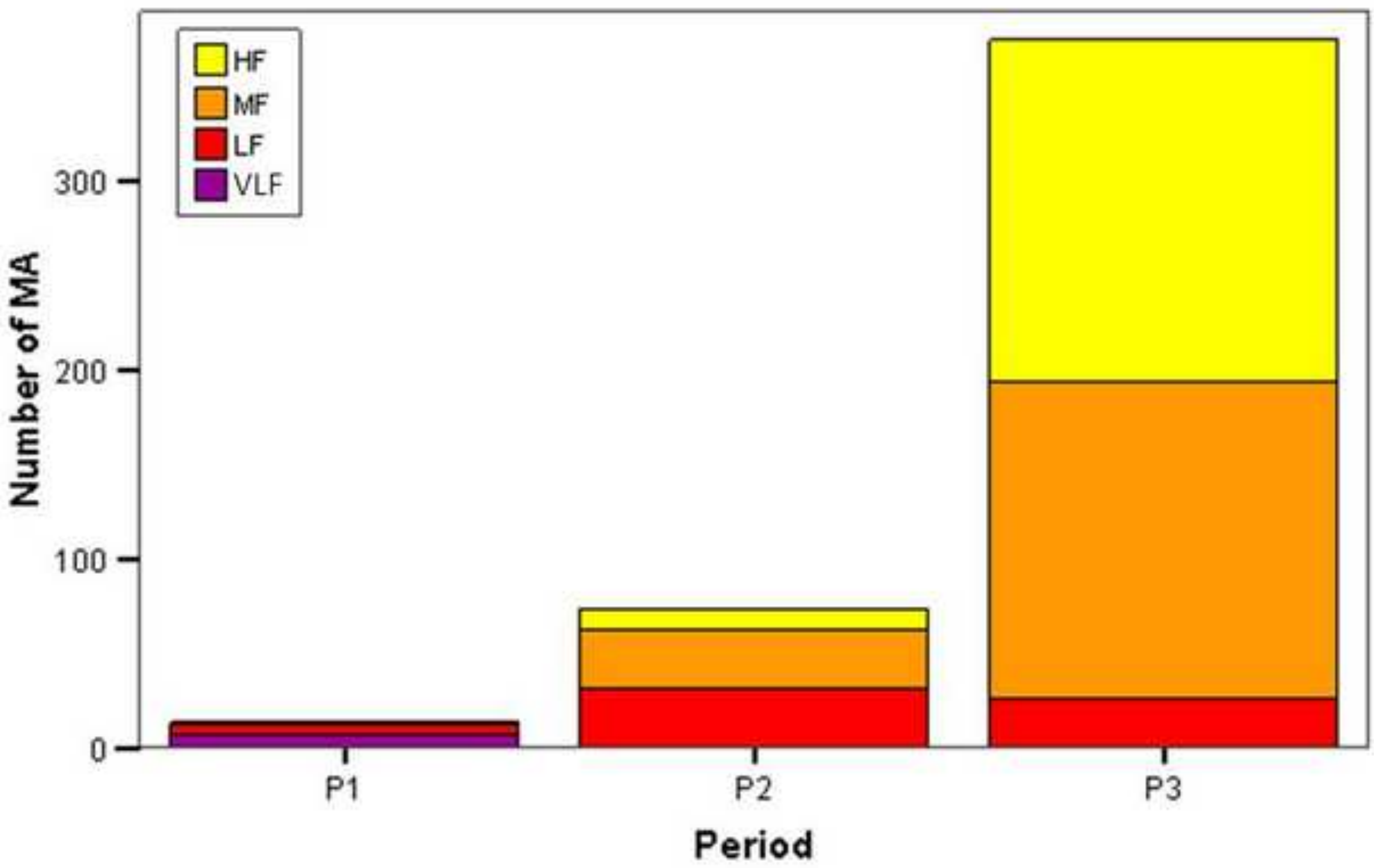

Figure(s)
Click here to download high resolution image

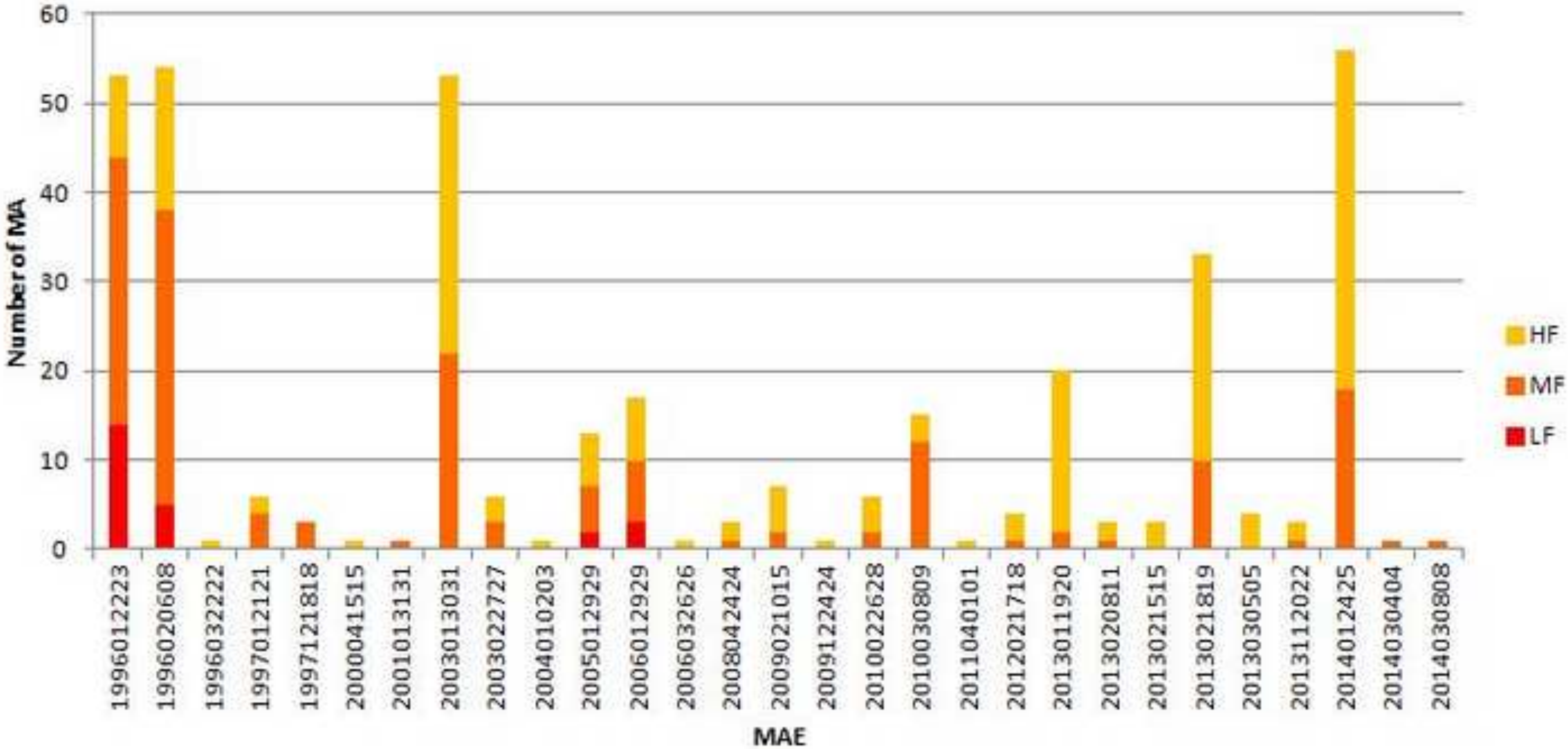

Figure(s)
Click here to download high resolution image

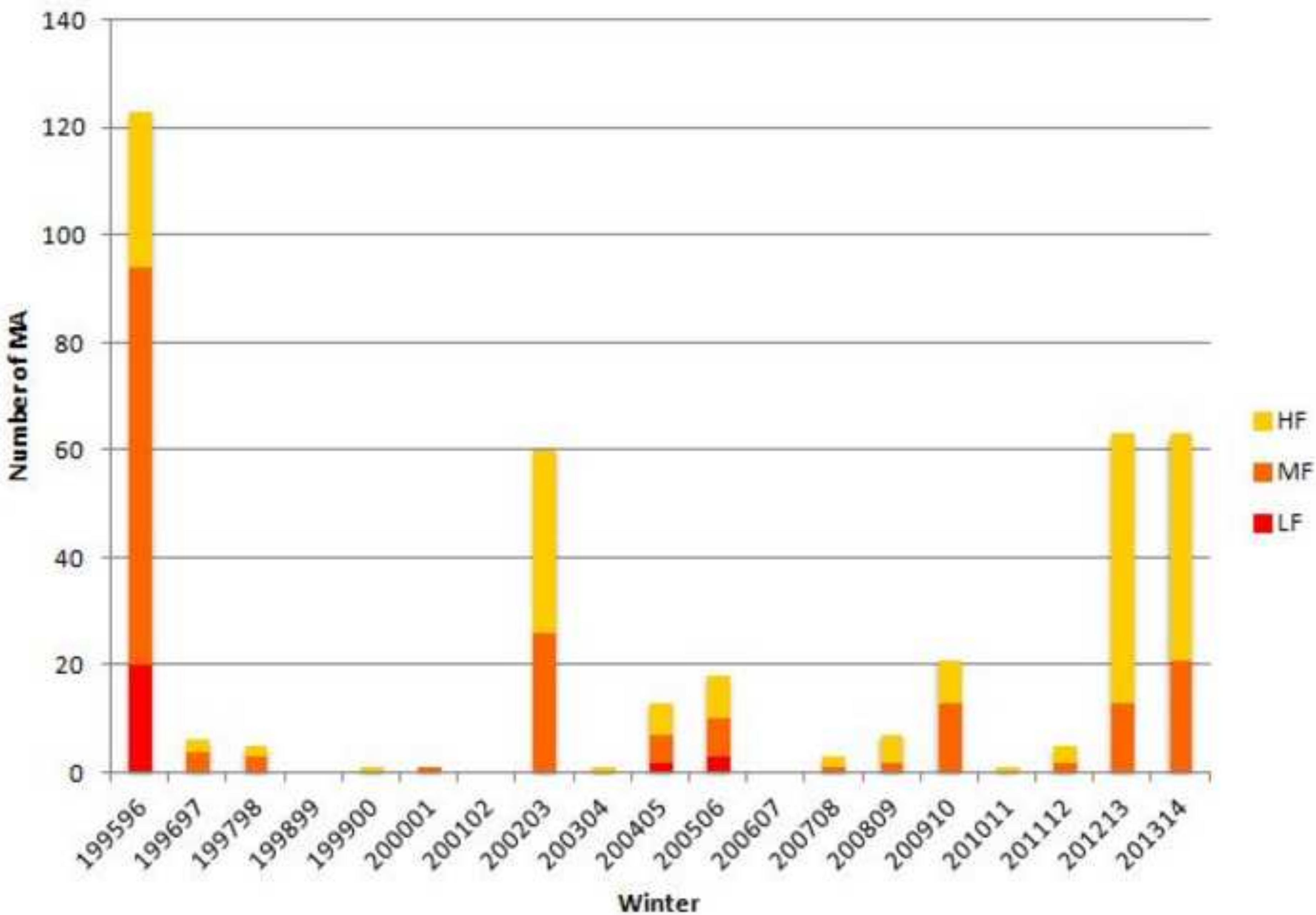

Figure(s)
Click here to download high resolution image

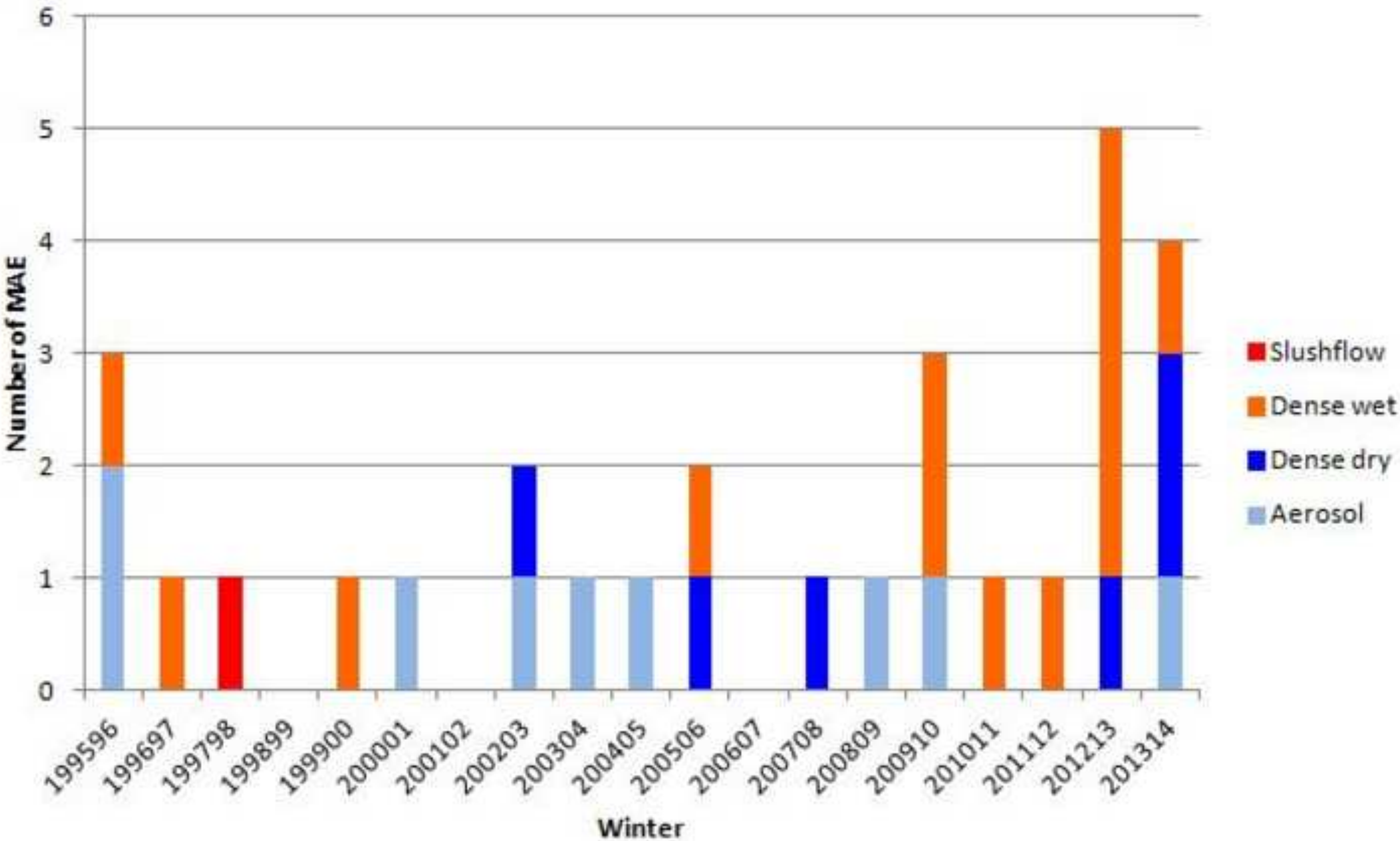

Figure(s)

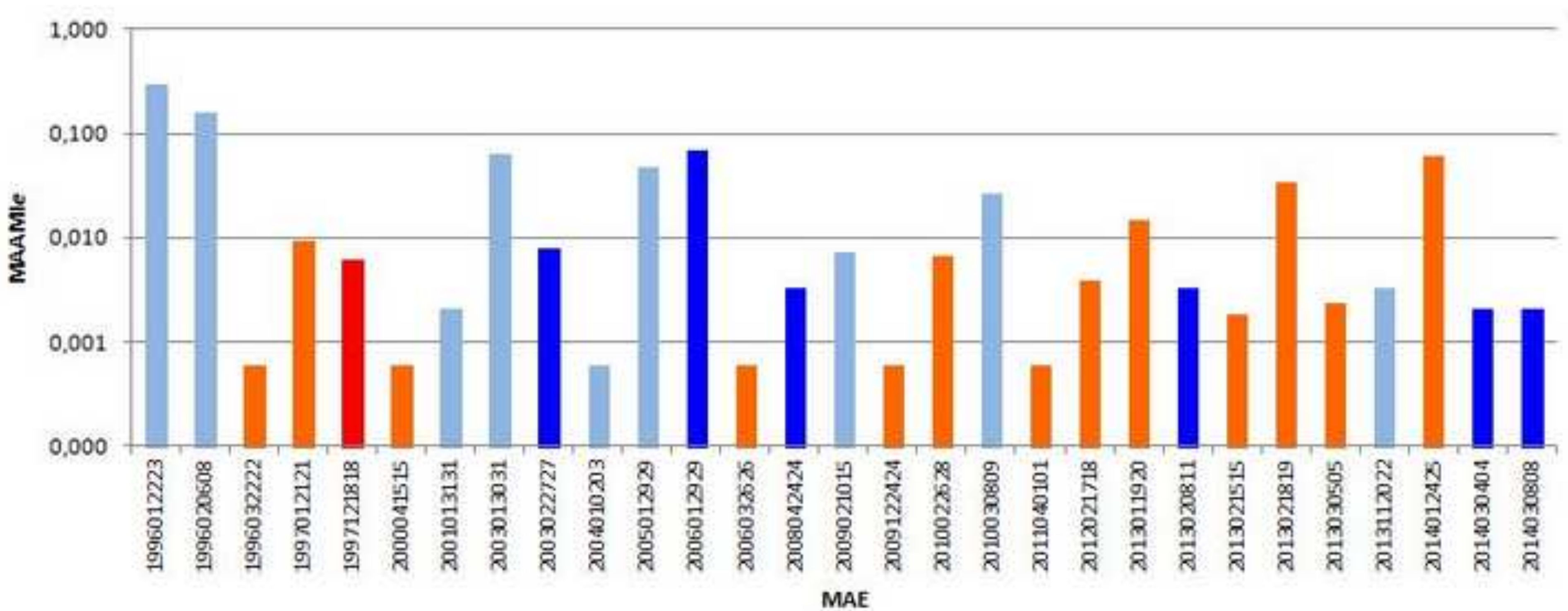
1,000
0,100
0,010
0,001
0,000
MAAMIe
1996012223
1996020608
1996032222
1997012121
1997121818
2000041515
2001013131
2003013031
2003022727
2004010203
2005012929
2006012929
2006032626
2008042424
2009021015
2009122424
2010022628
2010030809
2011040101
2012021718
2013011920
2013020811
2013021515
2013021819
2013030505
2013112022
2014012425
2014030404
2014030808
MAE

Figure(s)
Click here to download high resolution image

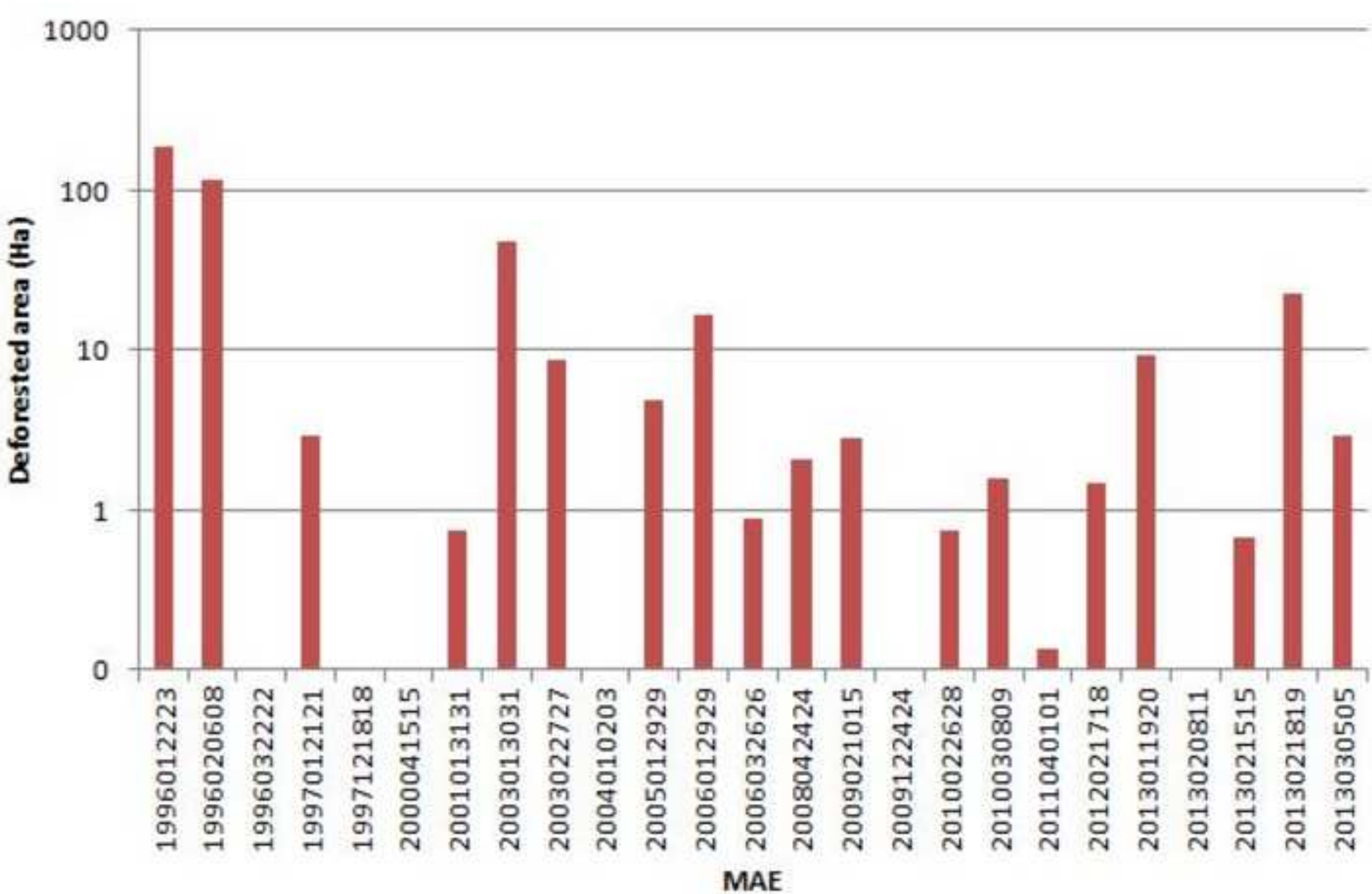

Figure(s)
Click here to download high resolution image

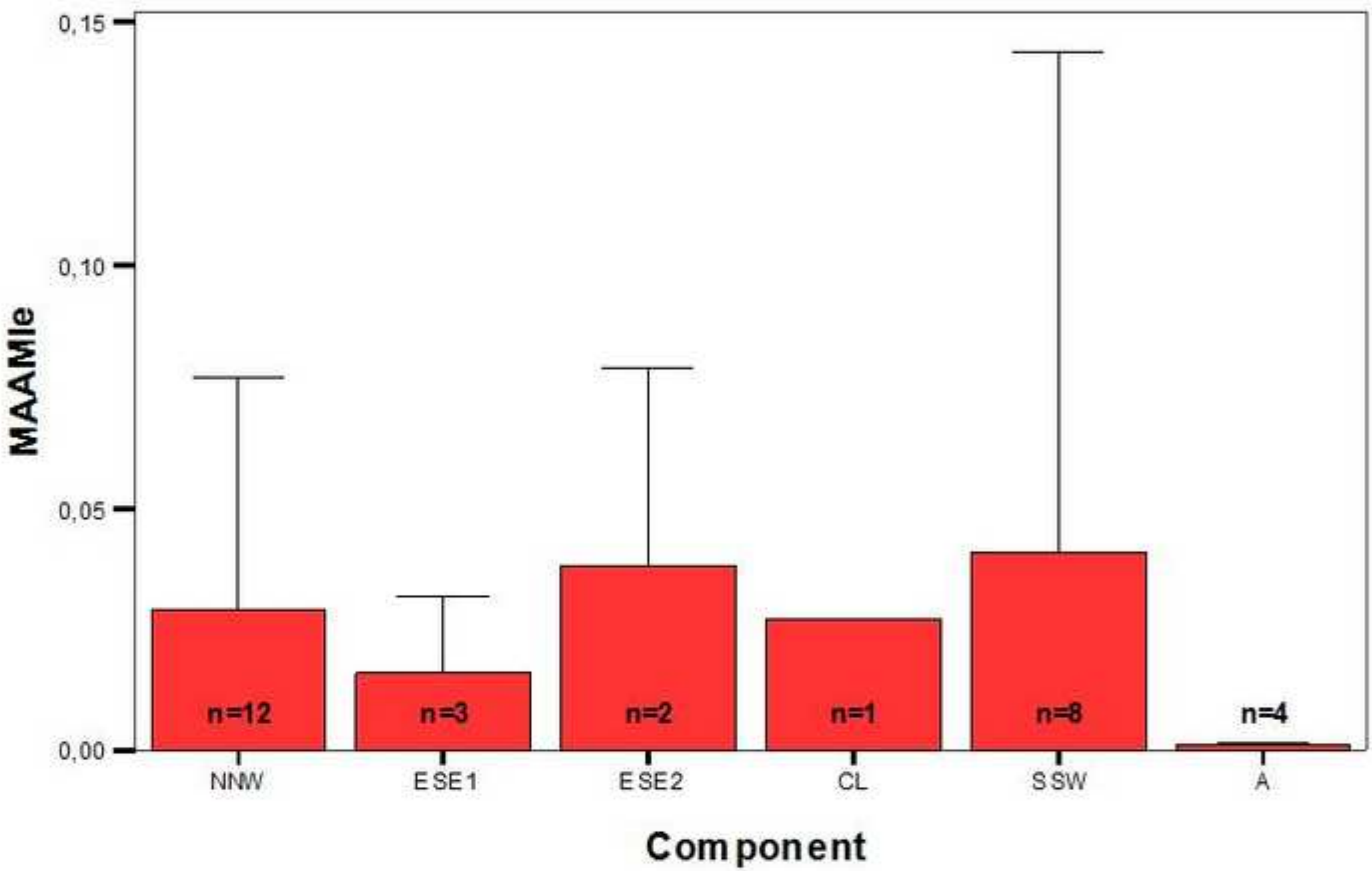

Figure(s)
Click here to download high resolution image

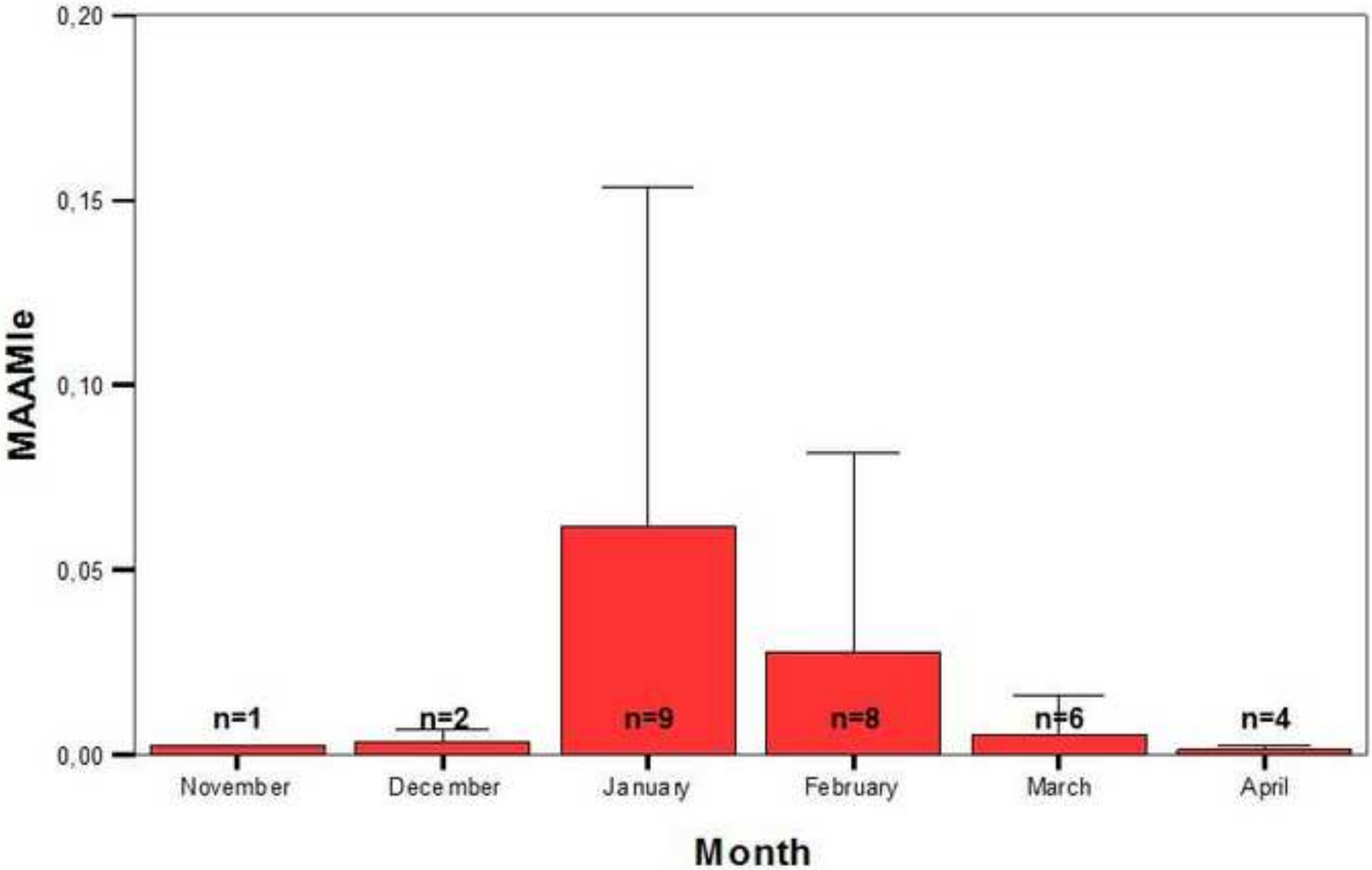

Figure(s)
Click here to download high resolution image

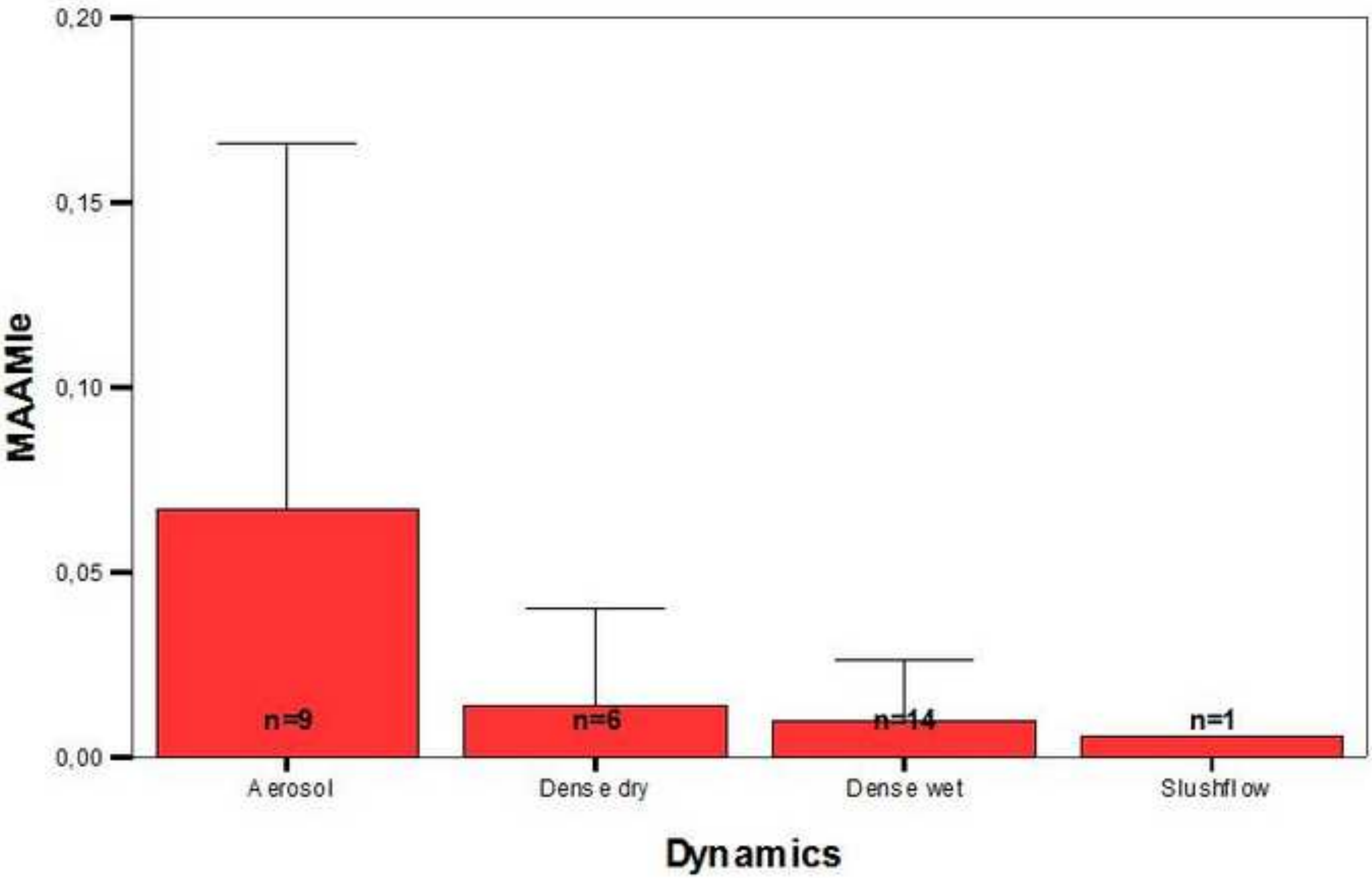

Figure(s)
Click here to download high resolution image

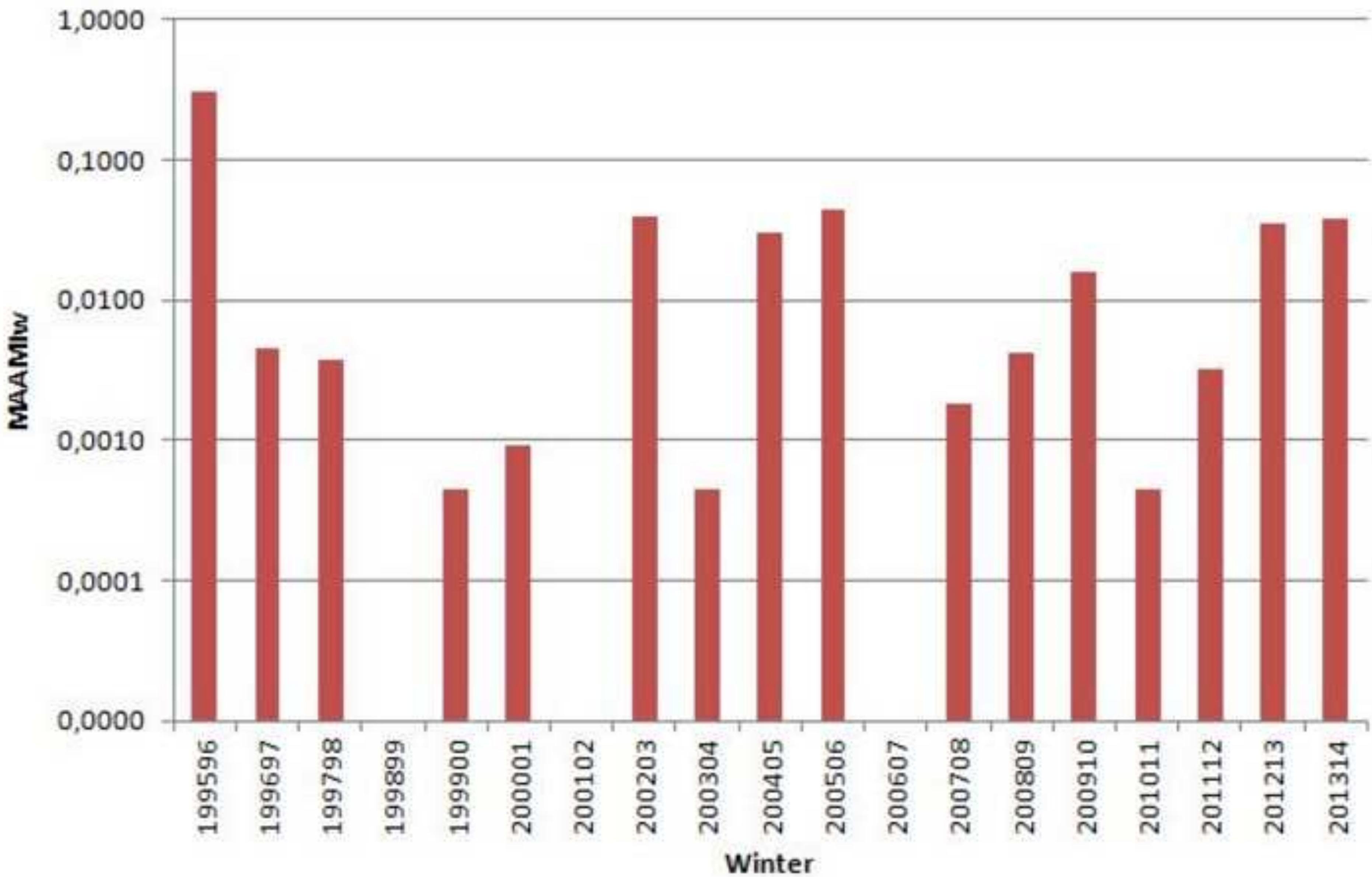

Figure(s)
Click here to download high resolution image

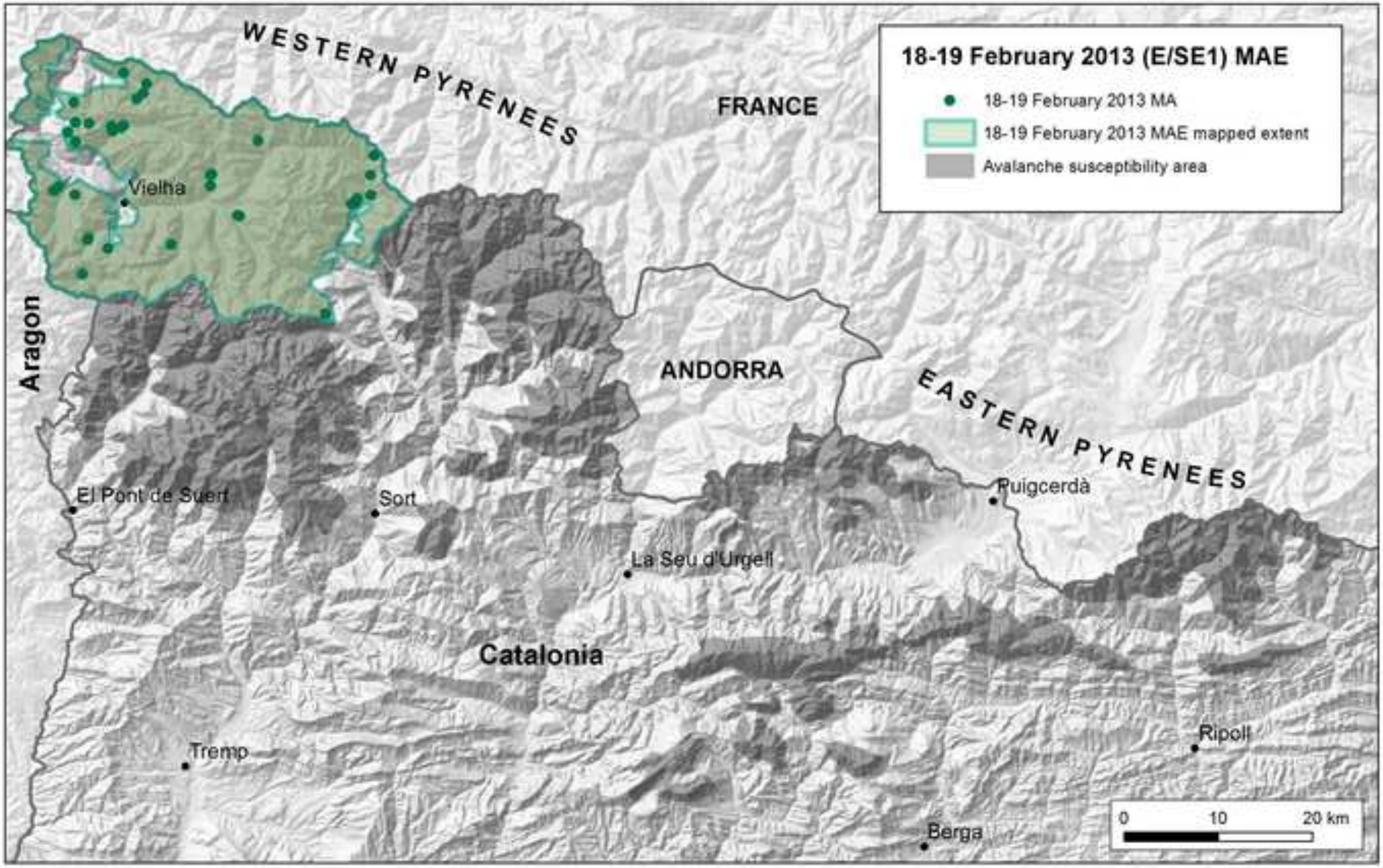

Figure(s)

Click here to download high resolution image

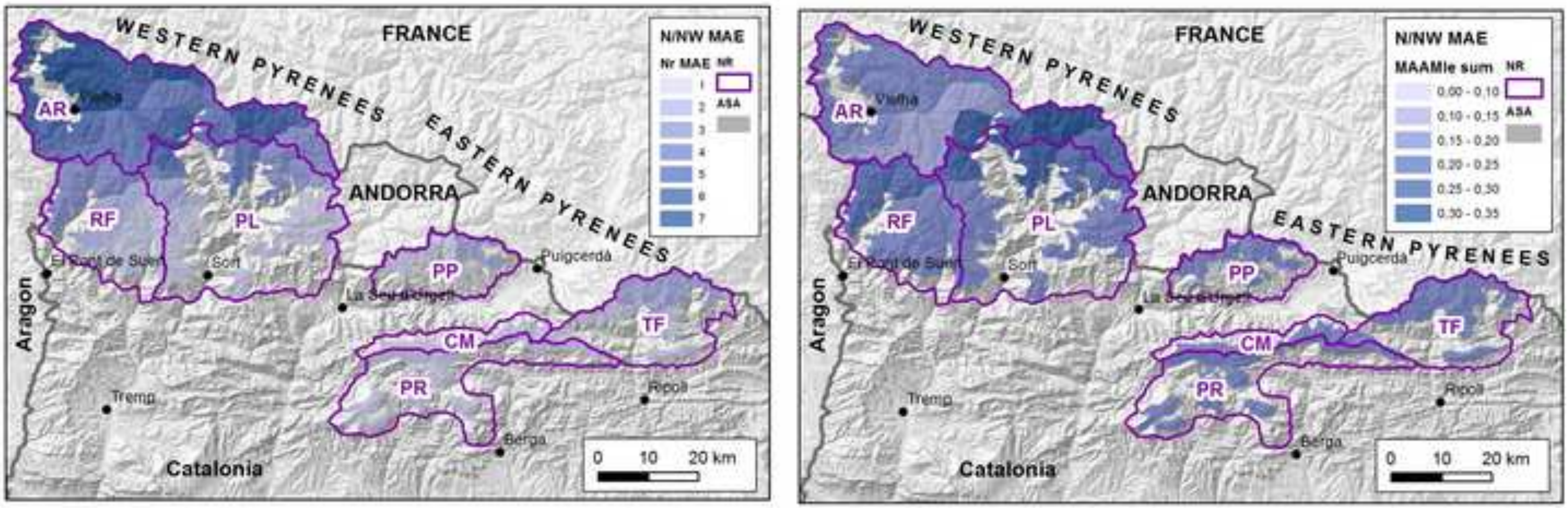

Figure(s)
Click here to download high resolution image

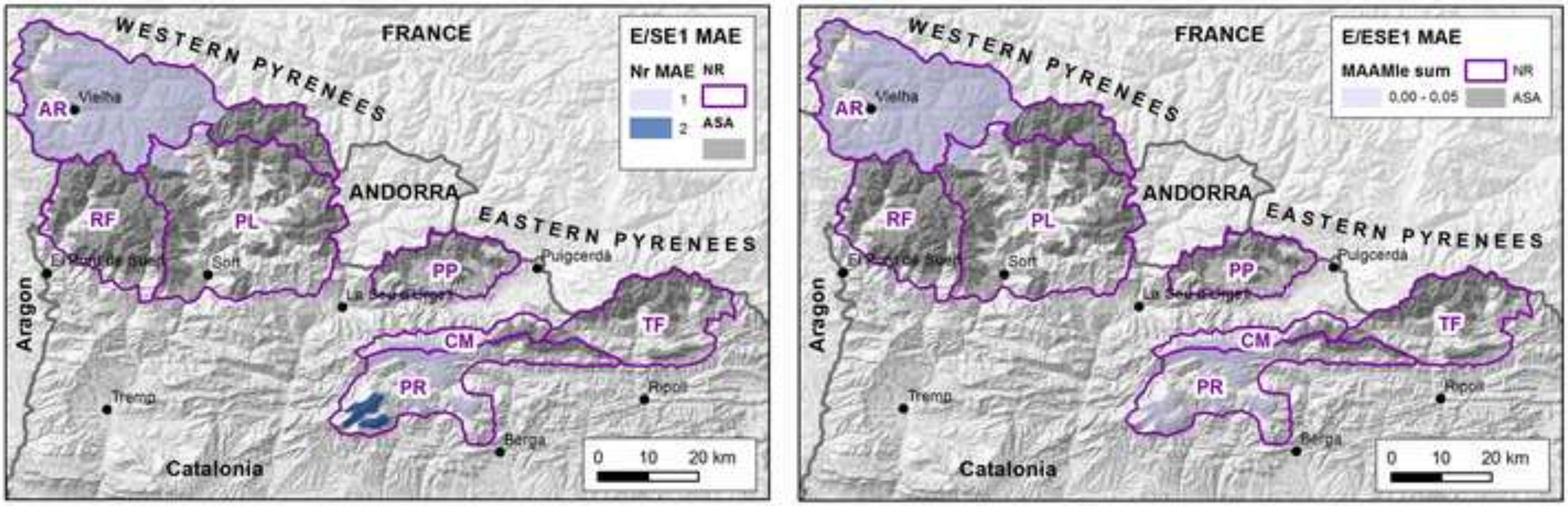

Figure(s)
Click here to download high resolution image

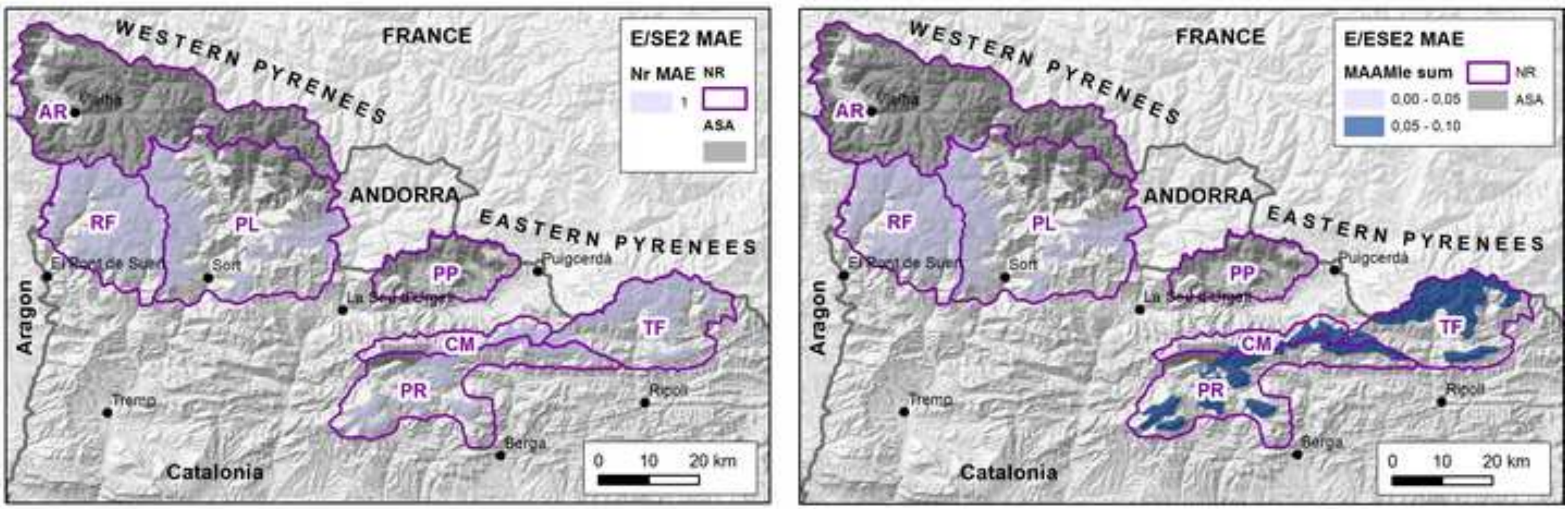

Figure(s)

Click here to download high resolution image

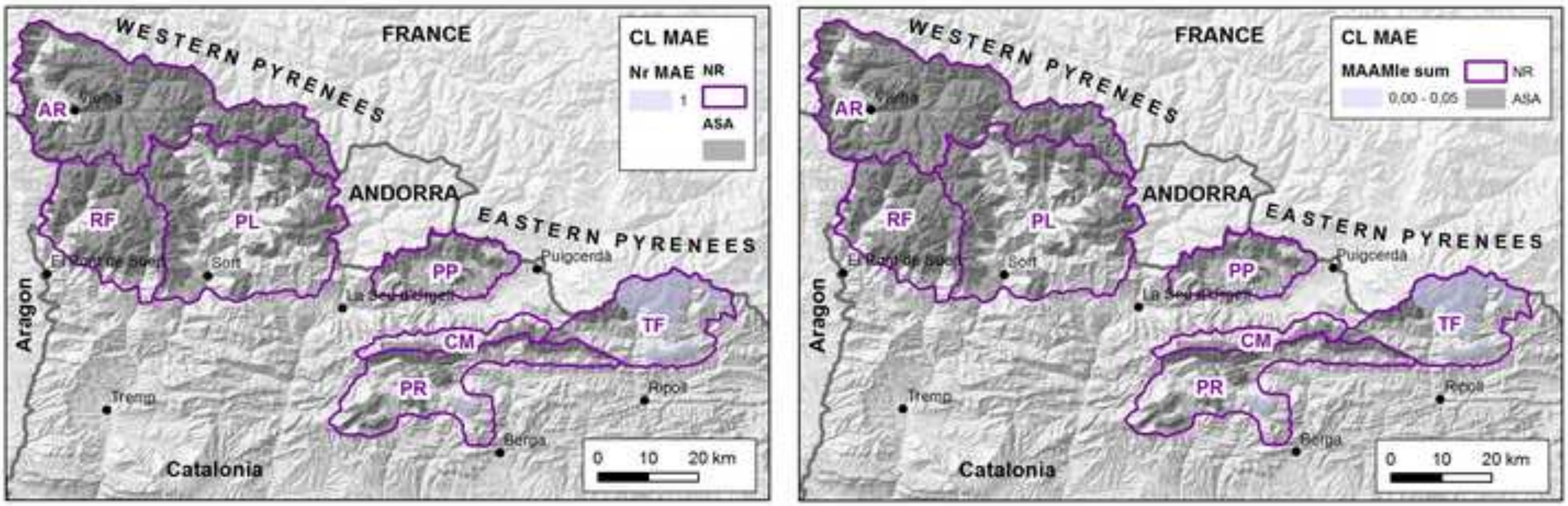

Figure(s)

Click here to download high resolution image

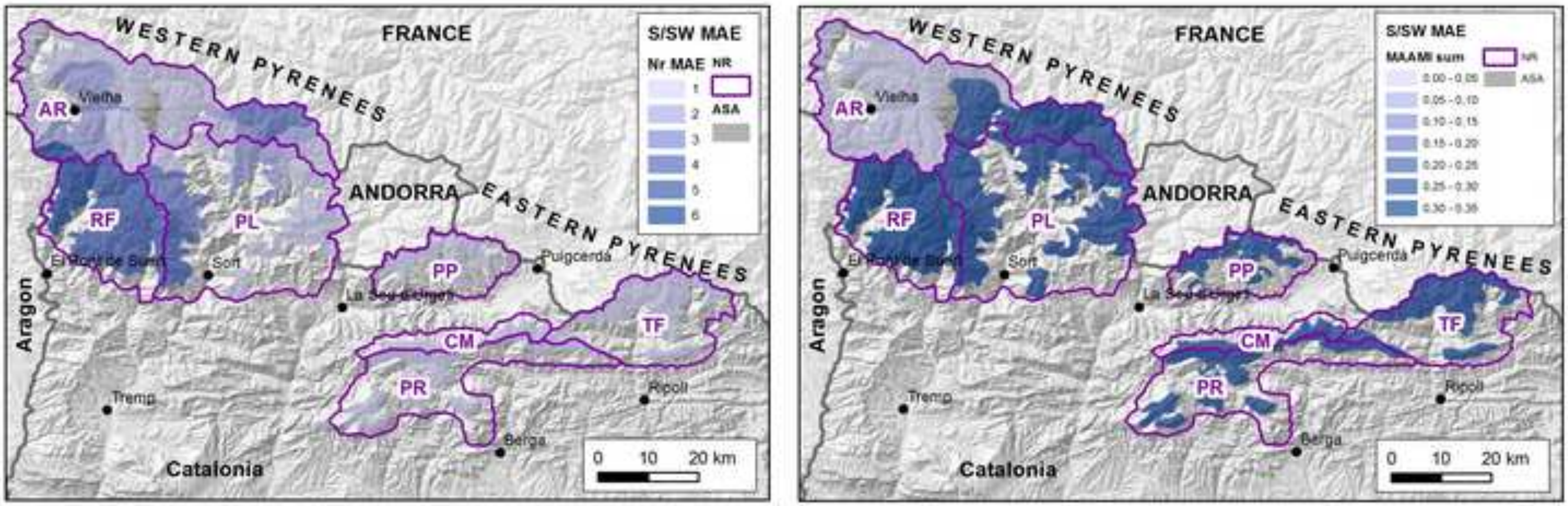

Figure(s)
Click here to download high resolution image

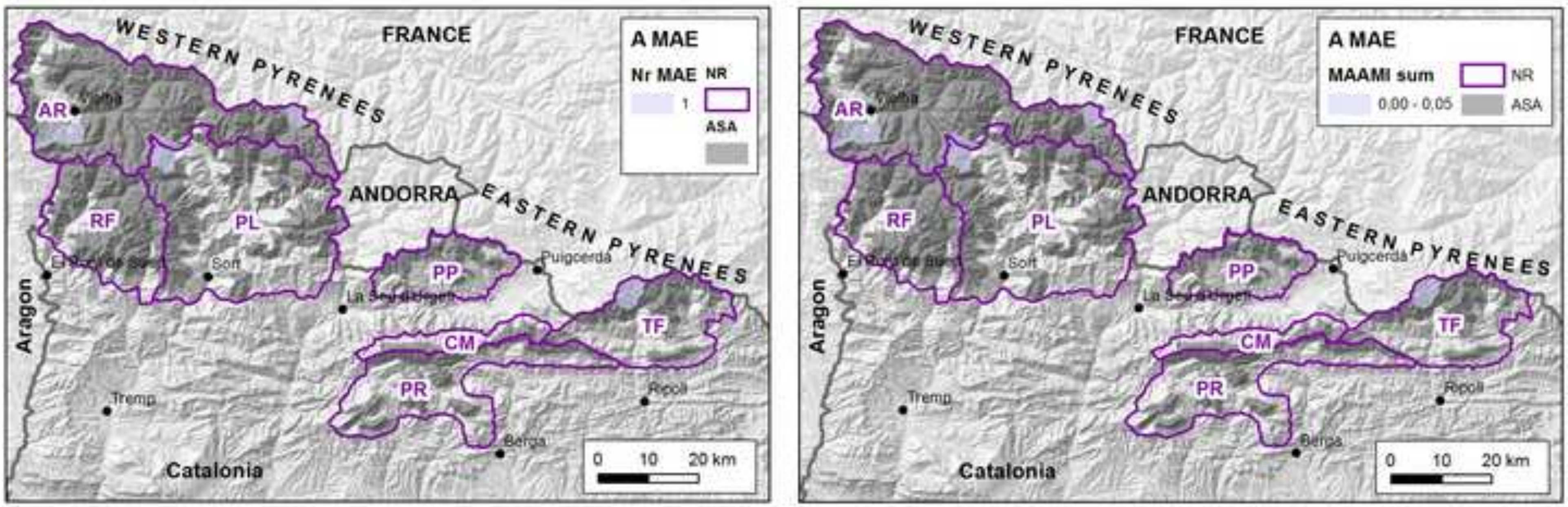

Figure(s)

Click here to download high resolution image

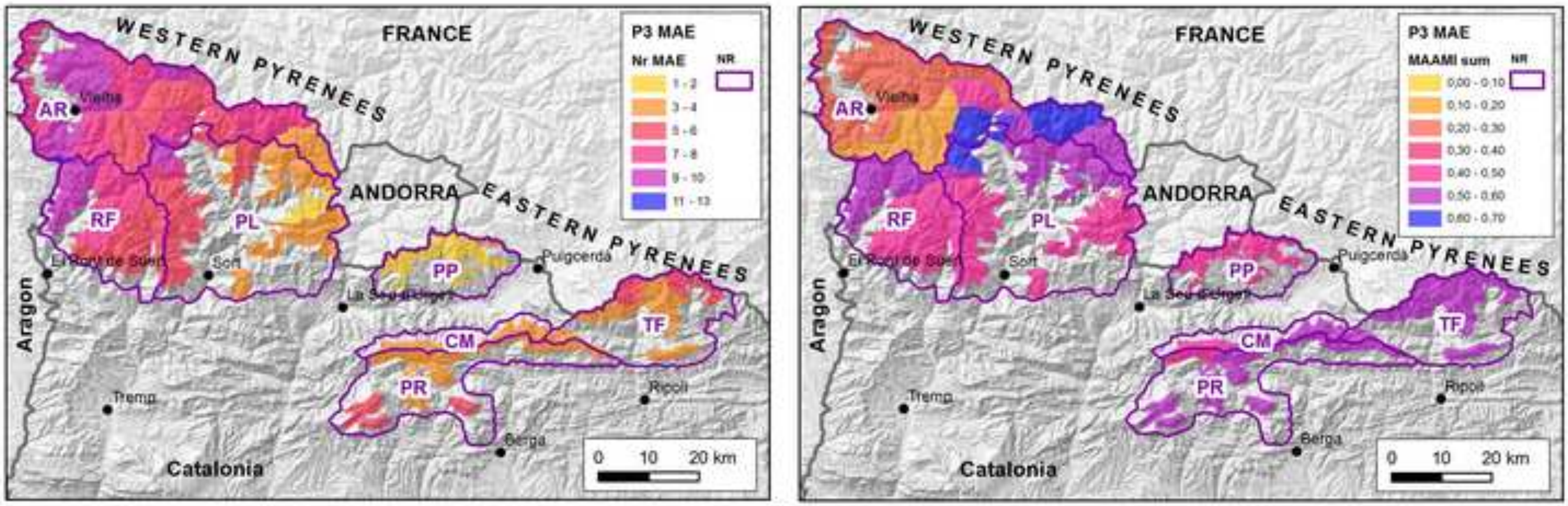

Figure(s)
Click here to download high resolution image

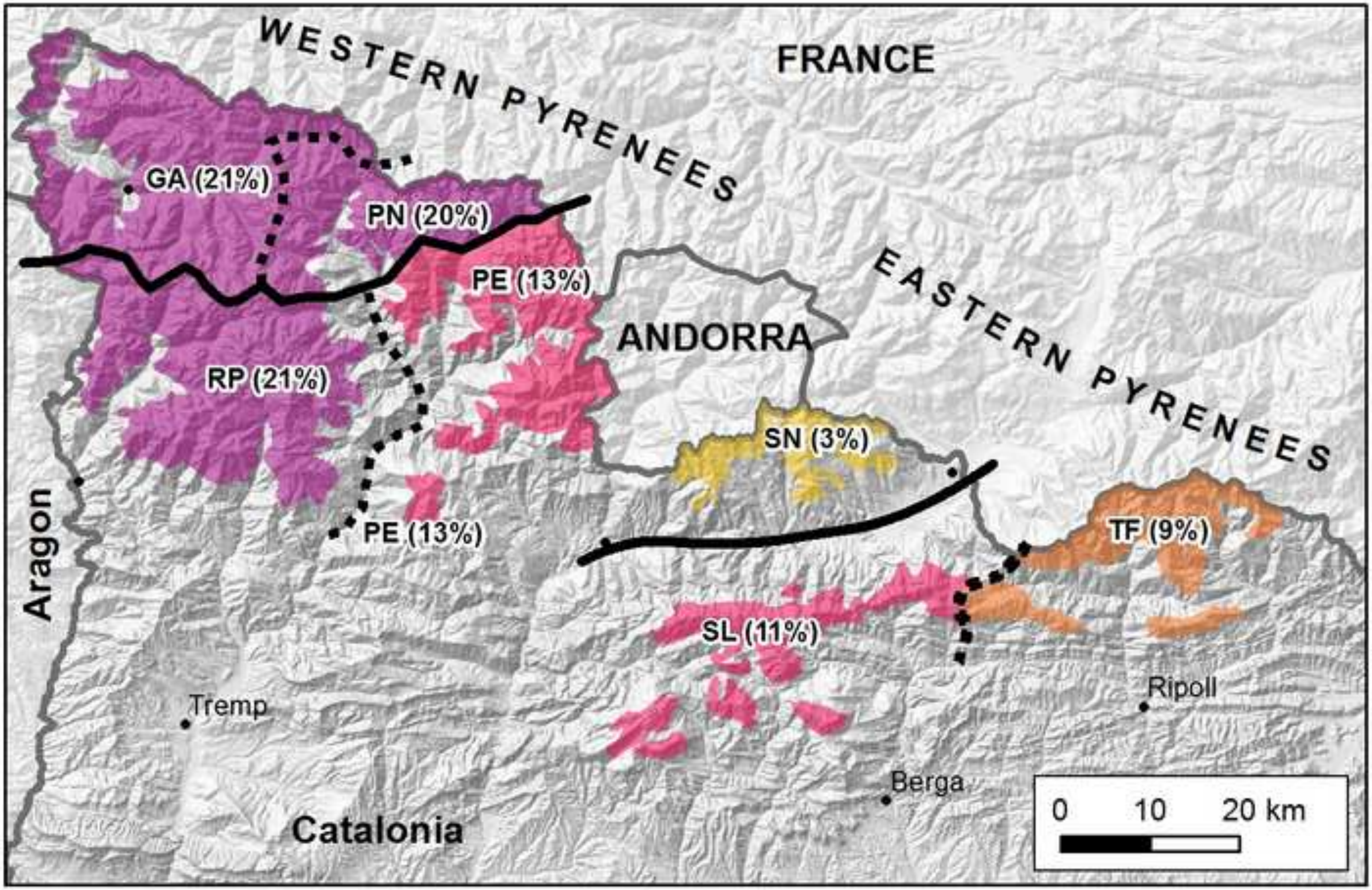

Figure(s)
Click here to download high resolution image

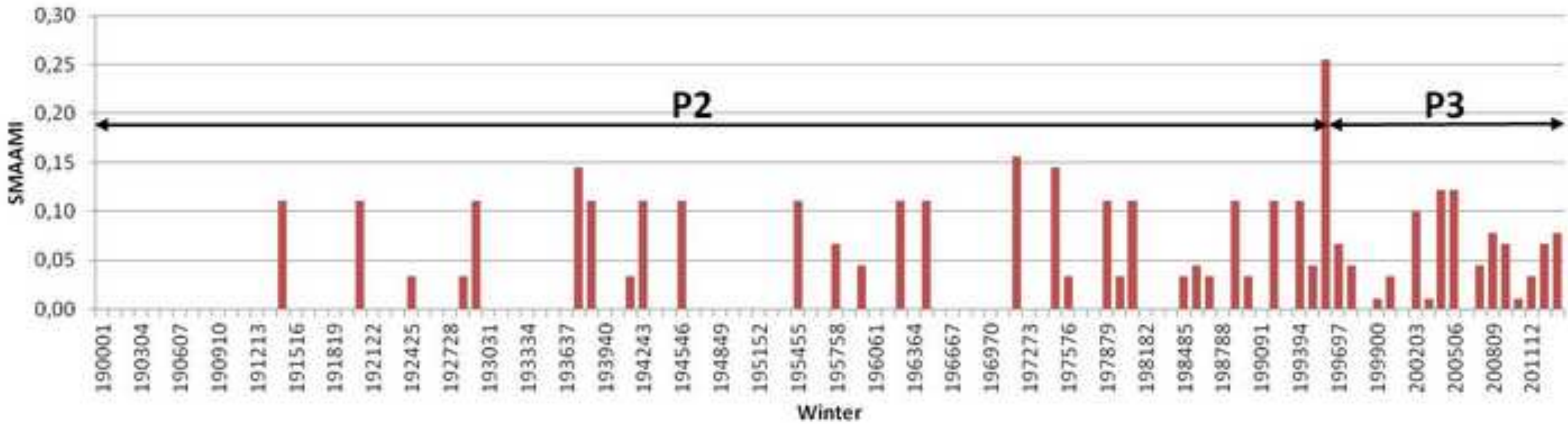

Figure(s)
Click here to download high resolution image

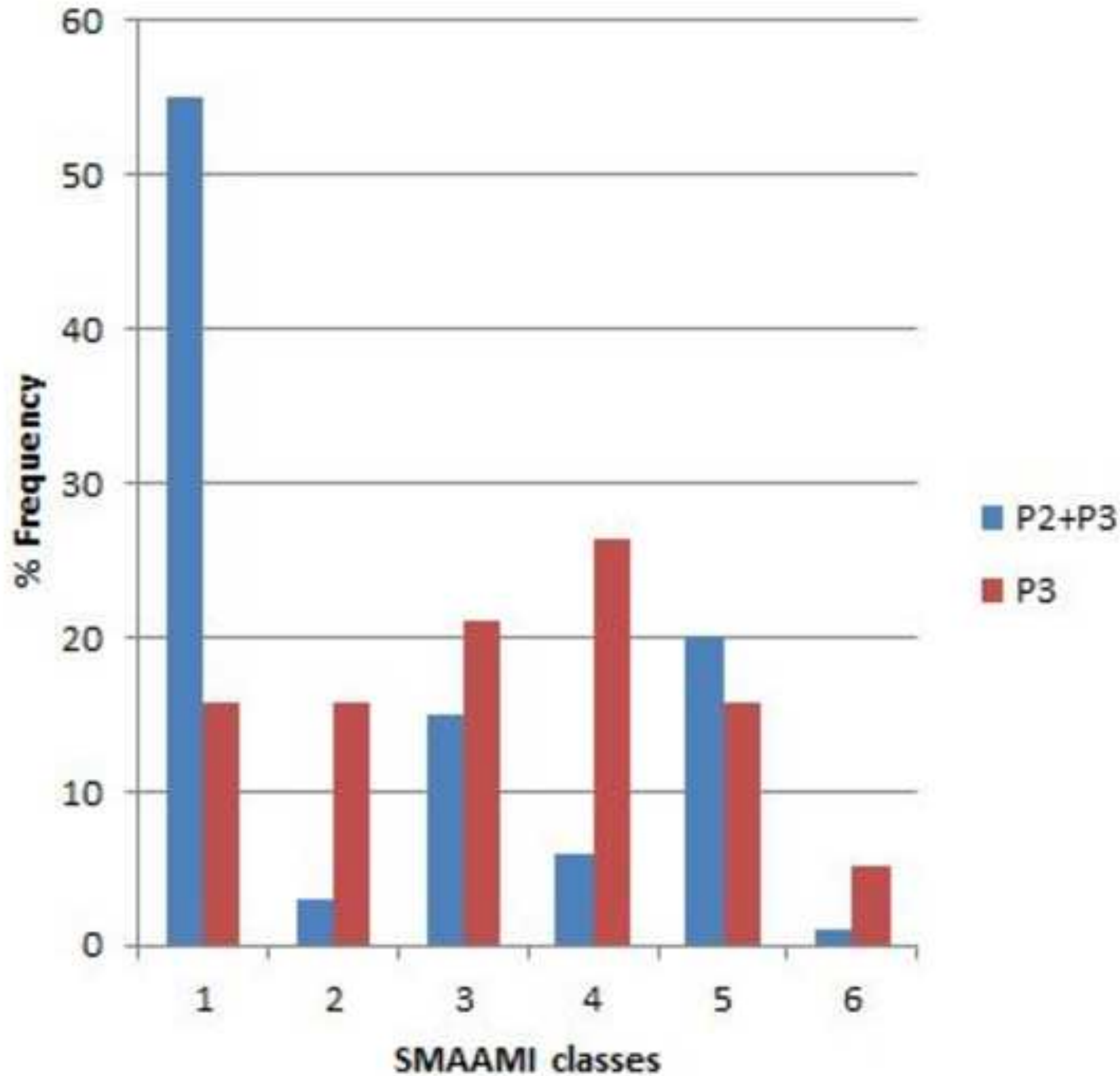

Figure(s)
Click here to download high resolution image

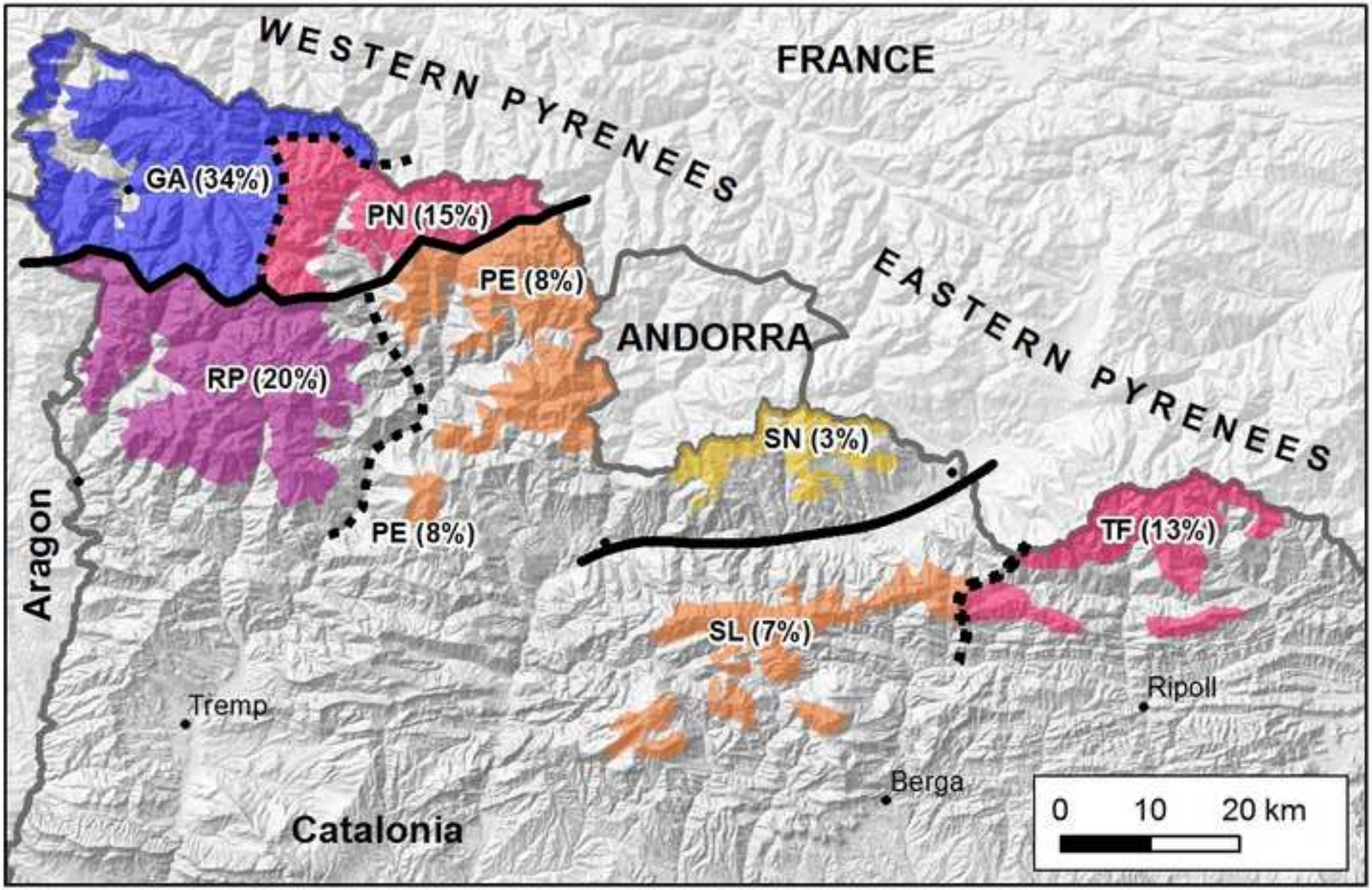

Figure(s)

Click here to download high resolution image